Altered X-chromosome inactivation predisposes to autoimmune manifestations in mice

Christophe Huret[1], Antoine David[2], Myriame Mohamed[1], Nicolas Valentin[3], Frédéric Charlotte[4], Michele Goodhardt[2], Claire Rougeulle[1,5] and Céline Morey[1,5]

[1] Université Paris Cité, CNRS, Epigenetics and Cell Fate, F-75013 Paris, France.

[2] Université Paris Cité, INSERM UMRS 976, Institut de Recherche Saint Louis, F-75010, Paris, France.

[3] Université Paris Cité, CNRS, Institut Jacques Monod, F-75013, Paris, France.

[4] Sorbonne University, Department of pathological anatomy and cytology, Hôpital Pitié-Salpêtrière Charles Foix, F-75013, Paris, France

[5] corresponding authors: claire.rougeulle@u-paris.fr; celine.morey@inserm.fr

Abstract

In mammals, males and females show marked differences in immune responses. Males are globally more sensitive to infectious diseases while females are more susceptible to systemic autoimmunity. X-chromosome inactivation (XCI), the epigenetic mechanism that ensures the silencing of one X in females, may participate in these sex-biases. To test this hypothesis, we perturbed the expression of the trigger of XCI, the non-coding RNA *Xist.* This resulted in exacerbated reactivation of X-linked genes of the Toll-like receptor 7 (*TLR7*) signalling pathway in monocyte/macrophages, dendritic cells and B cells during aging. Consequently, female mice spontaneously developed inflammatory signs similar, although milder, than those described in mouse models of lupus. Mechanistically, negative feedback of *TLR7* signalling is impaired in macrophages with perturbed XCI, leading to delayed restoration of basal transcriptional levels of target genes upon stimulation. These observations support a direct link between the regulation of XCI and female-biased autoimmune manifestations and highlight altered XCI as a potential cause of autoimmunity.

Introduction

In mammals, there is a marked sexual dimorphism in immune responses and functions. Males are significantly more sensitive to infections, while females are more susceptible to systemic autoimmune diseases[1,2]. This is partly explained by stronger innate and adaptative immunity in adult females, conferring a better response to various types of pathogens and vaccines compared to males. Such enhanced immunity may, however, lead to over-reactivity when not properly controlled, hence resulting in autoimmune manifestations. The determinants of this sexual bias are not fully understood. While these differences are partly attributable to sex hormones, X-linked factors represent other likely contributors[2–6]. Indeed, men with Klinefelter's syndrome, who bear an extra X-chromosome (47, XXY) in a male hormonal context, have a 10-15 higher risk of developing systemic lupus erythematosus (SLE) than women with Turner's syndrome, who have only a single X (45, XO) and female hormones[7,8]. Moreover, the onset of certain female-biased autoimmune diseases (Graves' disease, autoimmune hepatitis) may occur before puberty[9]. Incidentally, the X-chromosome has a high density of genes involved in immune functions[10,11] and some of these, including *TLR7*, *TASL*, *CXCR3 or CD40LG*, tend to be overexpressed in autoimmune conditions, suggesting a causal link between autoimmunity and X-linked gene regulation[3,6,7]. While the link between *Tlr7* overexpression and SLE has been firmly established – notably in the context of *Tlr7* transgenic male mice[12] and recently with the discovery of a *TLR7* gain-of-function mutation in a child with severe lupus[13] – how global modulation of X-chromosome expression impacts the fitness of the immune system is currently unknown.

X-linked gene expression is equalized between the sexes through the transcriptional silencing of most genes of one X chromosome, at random, in females. This X-chromosome inactivation (XCI) is an essential process established during early embryogenesis and maintained afterwards in daughter cells throughout *in utero* and postnatal life. XCI is triggered by the accumulation of *Xist* long non-coding RNA (lncRNA) on the inactive X (Xi) and recruitment of a series of factors inducing gene silencing in *cis*[14]. While in most cell types the repressed state is thought to be locked by several layers of chromatin modifications, XCI maintenance in immune cells exhibit certain special features. Firstly, a number of X-linked genes including *TLR7*, *TASL*, *CXCR3* tend to escape from XCI and are transcribed from the Xi in a significant proportion of immune cells in physiological conditions[4,8,10]. Secondly, Xi hallmarks including *XIST* accumulation and enrichment in repressive histone modifications H3K27me3/H2AK119ub are almost completely lost during B and T lymphopoiesis and regained upon lymphocyte activation[15]. These marks are very discrete or completely absent in NK cells, dendritic cells (DC) and macrophages (MΦ)[16]. This tendency is exacerbated in B lymphocytes from patients with SLE[15] or in stimulated B cells from the lupus mouse model

(NZB/W F1)[17,18]. These different patterns of XCI maintenance in immune cells are associated with specific *XIST* interactor networks in myeloid compared to lymphoid lineages, suggesting different regulatory requirements depending on immune cell[19]. Thirdly, knocking-out *Xist* when hematopoietic cells are specified results in differentiation defects during hematopoiesis, upregulation of natural XCI escapees[20] and aggressive blood cancer in adult mice[21], while it has relatively minor effects in other, non-immune, cell types[22,23]. In addition, *Xist* retains the ability to silence the X chromosome in immature hematopoietic precursor cells and not in hematopoietic stem cells or adult blood cells[24]. In human, repressing *XIST* in a B cell line results in increased expression of a subset of X-linked genes that tend to be overexpressed in atypical B cells (ABCs) of SLE patients[19]. Altogether, these findings suggest that XCI shows specific regulatory requirements/mechanisms in hematopoietic cells. However, whether these features provide female immune cells with higher adaptivity upon infection compared to male cells and/or whether such a unique functional plasticity may lead to over-reactivity of female immune system when not properly controlled remains to be formerly addressed[7].

In order to characterise the impact of perturbed X-linked gene regulation on immune functions *in vivo*, we used the *Ftx* KO background (*Ftx*$^{-/-}$) as a mean to impair XCI while bypassing lethality associated with *Xist* KO and mimic alterations that are susceptible to occur *in vivo*. *Ftx* is a non-coding gene of the X-inactivation centre (**Fig. 1a**), which acts as a *cis*-activator of *Xist* during the initiation of XCI[25,26]. Consequently, deletion of the *Ftx* promoter results in reduced *Xist* expression, impaired accumulation of *Xist* lncRNAs on the Xi and incomplete X-linked silencing during mouse ES cell differentiation[27], as well as during development in female mice[28,29]. Here we show that, in immune cells of *Ftx* KO females, XCI is progressively destabilised during aging resulting in the erosion of silencing of selected X-linked genes with immune functions. These include genes of the *TLR7* pathway for which escape from XCI is enhanced. This occurs coincidently with the development of autoimmune manifestations such as splenomegaly, higher percentages of activated lymphocytes and higher levels of natural antibodies in the blood. Mechanistically, macrophages of 1-year-old *Ftx* KO females are unable to properly restore normal levels of cytokine expression upon exogenous activation of the *TLR7* pathway, suggesting that this sub-efficient negative feedback generates an over-reactive immune environment. Altogether, these observations provide one of the first direct links between XCI deregulation – a female-specific biological process – and changes in immune cell features and point to XCI alteration as a potential trigger of various forms of autoimmune manifestations notably those affecting older women.

Results

<u>*Ftx* deletion induces aberrant *Xist* expression profiles in immune cells of adult females</u>

To study the effect of XCI perturbation on immune functions during adult life we created a mouse line carrying a deletion of *Ftx* transcription start sites similar to the mutations generated previously[27,29] (**Fig. 1a** and **SUP1a**). *Ftx* KO animals were born in Mendelian ratios (**SUP TABLE1**). Males and females developed normally, appeared healthy overall and fertile with no difference in life span compared to WT animals, as reported in[28,29]. As expected, *Ftx* expression was completely abolished in immune cells of *Ftx* KO females as measured by RT-qPCR (**SUP1b**) and by RNA-FISH (**SUP1c**). *Xist* expression appeared to be significantly reduced in *Ftx* KO immune cells (half the levels of WT) (**Fig. 1a**) and *Xist* lncRNAs hardly clustered on the Xi in immune cell nuclei from 3-months of age onwards (**Fig. 1b**). This indicates that *Ftx* deletion impacts *Xist* expression in adult immune cells. This perturbation can be considered as mild and likely results in mosaic cell populations constituted of cells showing variable degree of *Xist* alteration as illustrated by variable patterns of *Xist* lncRNA nuclear localisation (**Fig. 1b**). This probably allows cell-to-cell compensation therefore globally maintaining overall mouse fitness.

<u>Altered *Xist* expression results in overexpression and reactivation of several X-linked genes</u>

To determine if and how X-linked gene silencing is changed upon *Xist* perturbation, we measured the RNA levels of a battery of X-linked genes including immune-related and unrelated genes, housekeeping genes and genes known to escape from XCI using RT-qPCR on a selection of immune cell types of 3-month- and 1-year-old females (**Fig. 1c** and **SUP2**). At 3-months of age, no significant variation of X-linked RNA levels was observed between WT and mutant cells with the exception of *Xist,* as expected, and of *Cxcr3*, which was barely deregulated (**Fig. 1c and 1d**). In contrast, in 1-year-old females, a number of genes were significantly overexpressed in immune cells of *Ftx* KO vs WT (**Fig. 1c**). Interestingly, many of these genes (*Tlr7*, *Tlr8*, *Tasl/CXorf21*, *Cybb* and *Cxcr3*) naturally escape from XCI in a significant proportion of immune cells[30]. Examination of RNA levels in individual mice showed high animal to animal variability (**Fig. 1d**), which may reflect variable frequencies of cells in which XCI was not properly established in the hematopoietic stem population.

Overexpression may result from higher expression of alleles on the active X, from increased expression of alleles that escaped XCI in these cells or from extended re-activation of Xi alleles to additional cells, which means, in this latter configuration, a relaxation of XCI-mediated silencing of these genes. To discriminate between these possibilities, we performed double RNA-FISH for *Tlr7* and *Xist* or for *Tasl* and *Xist* on Monocyte/Macrophages (Mo/MΦ) from the

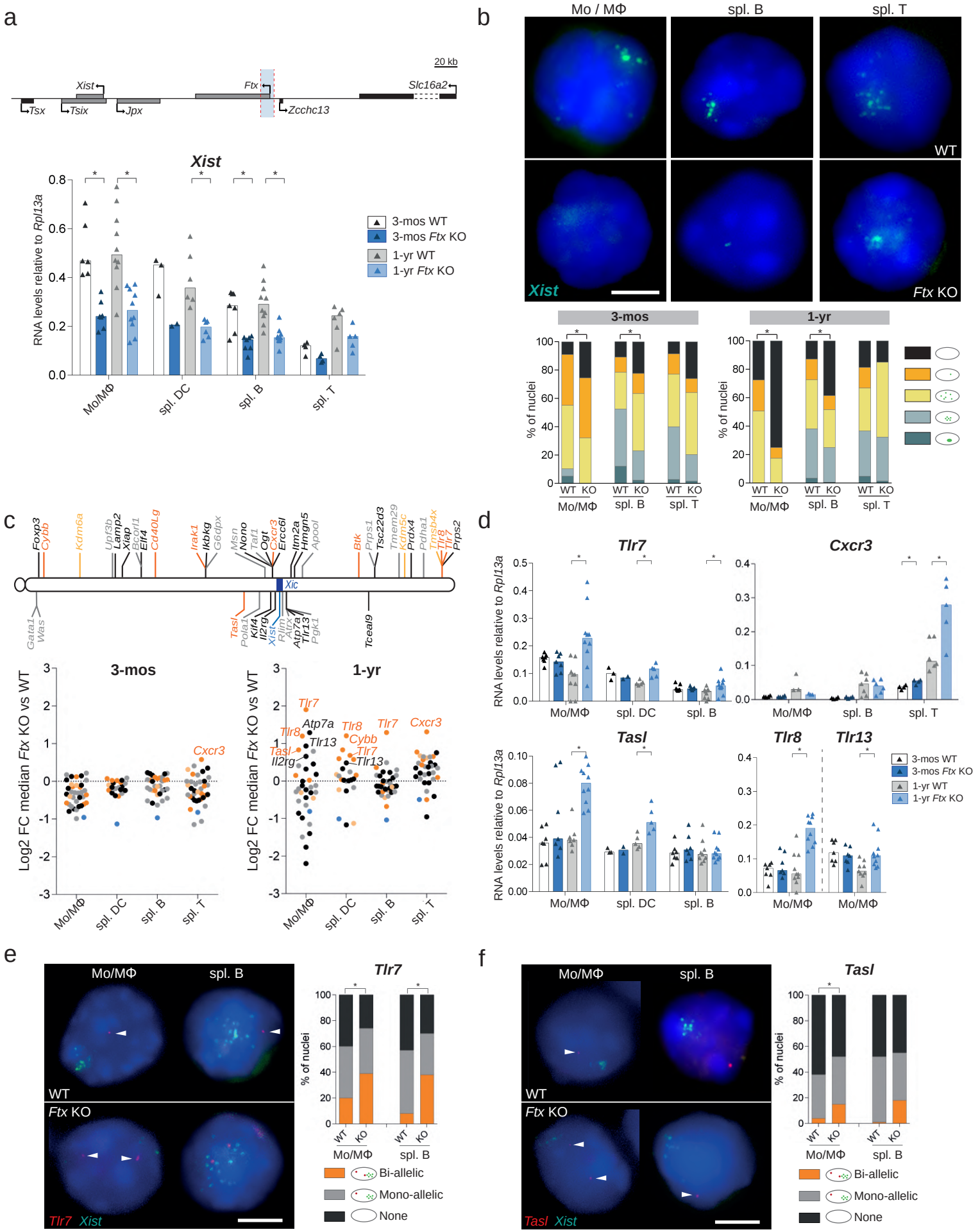
a
20 kb
Xist
Ftx
Slc16a2
Tsx
Tsix
Jpx
Zcchc13
Xist
RNA levels relative to Rpl13a
3-mos WT
3-mos Ftx KO
1-yr WT
1-yr Ftx KO
Mo/MΦ
spl. DC
spl. B
spl. T
b
Mo / MΦ
spl. B
spl. T
WT
Xist
Ftx KO
3-mos
1-yr
% of nuclei
WT KO
Mo/MΦ
spl. B
spl. T
c
Foxp3
Cybb
Kdm6a
Upf3b
Lamp2
Xiap
Bcorl1
Elf4
Cd40Lg
Irak1
Ikbkg
G6dpx
Msn
Nono
Taf1
Ogt
Cxcr3
Ercc6l
Itm2a
Hmgn5
Apool
Btk
Prps1
Tsc22d3
Tmem29
Kdm5c
Prdx4
Pdha1
Tmsb4x
Tlr8
Tlr7
Prps2
Xic
Gata1
Was
Tasl
Pola1
Kif4
Il2rg
Xist
Rlim
Atrx
Atp7a
Tlr13
Pgk1
Tceal9
3-mos
1-yr
Log2 FC median Ftx KO vs WT
Cxcr3
Tlr7
Atp7a
Tlr8
Tlr13
Cybb
Tlr7
Cxcr3
Tlr8
Tasl
Il2rg
Tlr7
Tlr13
Mo/MΦ
spl. DC
spl. B
spl. T
d
Tlr7
Cxcr3
RNA levels relative to Rpl13a
Mo/MΦ
spl. DC
spl. B
spl. T
Tasl
Tlr8
Tlr13
3-mos WT
3-mos Ftx KO
1-yr WT
1-yr Ftx KO
e
Mo/MΦ
spl. B
WT
Ftx KO
Tlr7 Xist
Tlr7
% of nuclei
WT KO
Mo/MΦ
spl. B
Bi-allelic
Mono-allelic
None
f
Mo/MΦ
spl. B
WT
Ftx KO
Tasl Xist
Tasl
% of nuclei
WT KO
Mo/MΦ
spl. B
Bi-allelic
Mono-allelic
None

Figure 1

Figure 1. Perturbation of X-inactivation in immune cells of *Ftx* KO females results in overexpression of several X-linked genes associated with autoimmune conditions.

- **a.** Map of the X inactivation center showing the location of *Xist*, *Ftx* and the *Ftx* promoter region that has been deleted (blue shading). Underneath, *Xist* RNA levels measured by RT-qPCR in wild-type (WT) and *Ftx* KO females at 3-months (3-mos) and 1-year (1-yr) of age. Each triangle represents RNA levels in a mouse. Bar plots show median values. (*t-test*, **p*-values < 0.05). In this figure, Monocytes/macrophages (Mo/MΦ) were collected from the bone marrow. Other cells types were collected from the spleen.
- **b.** Representative images of RNA-FISH for *Xist* (green) on wild type and *Ftx* KO female cells in the indicated cell type. The percentages of cells with different patterns of *Xist* RNA distribution in the cell populations are shown on the histograms. (Fisher's exact test, **p*-values < 0.05, N > 2 mice, n > 100 nuclei). Scale bar, 5μm. Note that *Xist* lncRNAs tend to be delocalized from the Xi even in WT mice as previously described[15].
- **c.** Map of the X chromosome showing genes known to constitutively escape from XCI (yellow), genes with immune function and a tendency to escape from XCI (orange), other genes with immune function (black) and housekeeping genes (grey). Underneath, log2 fold change between median RNA levels as measured by RT-qPCR in KO versus WT mice for each gene, in the indicated cell type, either in 3-month- (left) or in 1-year-old mice (right). Each dot represents an X-linked gene. The names of genes showing significantly different RNA levels between KO vs WT are indicated on the graphs. (*t-test*, *p*-values *< 0.05; n ≥ 3 mice per genotype)
- **d.** RNA levels of *Tlr7*, *Cxcr3*, *Tasl*, *Tlr8* and *Tlr13* as measured by RT-qPCR in cell types showing detectable expression. Each triangle represents RNA levels in a mouse. Bar plots show median values. (*t-test*, **p*-values < 0.05).
- **e.** Representative images of RNA-FISH for *Tlr7* (red) and *Xist* (green) on WT and *Ftx* KO cells from 1-year old female mice. Scale bar, 5μm. The percentages of cells with bi-allelic, mono-allelic or no signals are shown on the histogram.
- **f.** Same as panel **e** for *Tasl* transcription.

bone marrow (BM) of 1-year-old females, in which the differential of expression in *Ftx* KO vs WT by RT-qPCR is most pronounced (**Fig. 1d**). We detected significantly higher percentages of nuclei with two pinpoint signals indicating active primary transcription sites on each X chromosome in *Ftx* KO compared to WT cells (**Fig. 1e and 1f**). These profiles indicate bi-allelic expression and therefore escape from XCI of *Tlr7* or *Tasl* Xi copies and indicate that this phenomenon is amplified in 1-year-old *Ftx* KO Mo/MΦ compared to WT. Similar bi-allelic expression is observed in B cells from 1-year-old mice (**Fig. 1e and 1f**).

Not all known natural escapees however appeared overexpressed (**SUP2a**) while some genes supposedly subject to XCI (*Tlr13*, *Il2rg* and *Atp7a*) showed higher RNA levels in *Ftx* KO compared to WT cells (**Fig. 1c**, **1d** and **SUP2b**) suggesting that labile expression from the Xi may facilitate – but is not a prerequisite for – overexpression. In contrast, expression of X-linked housekeeping genes was not significantly perturbed in *Ftx* KO immune cells (**SUP2c**). We also observed some genes with lower expression in *Ftx* KO cells compared to WT (**Fig. 1c** and **SUP2d**). While these changes did not reach significance, they may constitute secondary targets of X-linked gene overexpression.

Altogether, these results indicate that the perturbation of *Xist* expression in *Ftx* KO immune cells does not lead to global reactivation of the Xi but rather to specific local reactivation or enhanced escape from XCI of specific X-linked genes. Apart from *Cxcr3*, overexpression is not detected before 1-year of age (**Fig. 1c** and **1d,**) suggesting a progressive loss of silencing with age at these loci in a growing number of immune cells.

<u>X-linked genes overexpressed upon XCI perturbation are enriched in factors associated with autoimmune phenotypes</u>

The most striking feature of X-linked genes affected by *Xist* perturbation is the preponderance of genes involved in innate immune response (*TLR7*, *TLR8*, *TLR13*, *TASL* and *CXCR3*), which have been reported to be associated with or to have a causative role in different autoimmune diseases (**SUP TABLE2**)[12,13,31–33]. They include many membrane receptors present at the lysosome surface (*TLR7*, *TLR8*, *TLR13*) or at the plasma membrane (*CXCR3*). No significant deregulation of two other membrane receptor genes, *Il4ra* and *Il6ra,* that are located on autosomes could be detected in *Ftx* KO immune cells, which confirms a specific effect on X-linked receptors (**SUP3a**). *TLR7*, *TLR8* and *TLR13* trigger, upon activation, the NF-κB pathway[34] but neither *Irak1* nor *Ikbkg* (NEMO), two X-linked core effectors of this pathway[34], showed significant change in their expression level in *Ftx* KO immune cells (**SUP3b**). This suggests either that they are not sensitive to *Xist* perturbation or that they are under the control of additional regulations as they occupy a central position in a signalling cascade which may be activated by many different cues.

Female mice with impaired XCI develop a splenomegaly during aging

To characterise changes in the immune system upon XCI perturbation and test whether innate immunity may be increased, we looked for signs of inflammation in *Ftx* KO female mice. We first examined the spleen at 3-months of age and could not detect any difference in spleen weight or morphology between *Ftx* KO and WT females (**Fig. 2a**). In contrast, spleens from 1-year- and, more drastically, from 2-year-old females appeared significantly larger in *Ftx* KO conditions (**Fig. 2a**). Histological analyses did not reveal any defects in cell organisation, any signs of fibrosis or of cell infiltration in *Ftx* KO spleens compared to WT at any age (**Fig. 2b** and **SUP4a**). Both the time-course progression of the splenomegaly and the fact that it never occurred in males (**SUP4b**) are consistent with XCI molecular alterations that we observed.

Flow cytometry analysis of main splenic cell populations (B, T, myeloid, dendritic and erythroid cells) using cell surface markers revealed that the increase in splenic cell count in 1-year-old KO females resulted from a multilineage cell expansion preferentially targeting myeloid and dendritic cells while B cell percentages appear, comparatively, reduced (**Table 1**). No differences were observed between aged-matched *Ftx* KO and WT males (**SUP TABLE3**).

We then defined the sub-populations of splenic B, myeloid and dendritic cells impacted by XCI perturbation in 1-year-old KO females. All types of splenic B cells including marginal zone (MZ) B cells, follicular and transitional B cells appeared reduced in percentages (**Table 1**) while percentages of both myeloid (m-DC) and plasmacytoid (p-DC) dendritic cells (**Fig. 2c**) and of Mo/MΦ were higher in *Ftx* KO compared to WT animals (**Table 1**).

To determine whether the splenic defects may originate in the bone marrow, we monitored the distribution of the main hematopoietic lineages together with that of precursors including hematopoietic stem progenitor cells (HSPC) and B committed progenitors at various ages. No significant differences either in the hematopoietic stem compartment, in T, myeloid or erythroid committed cells could be detected between *Ftx* KO and WT females (**SUP TABLE4**). In the B lineage, we observed a significant reduction of the percentage of $CD19^+$ B cells in 2-year-old *Ftx* KO females compared to WT together with a global deregulation of B cell differentiation. The B cell compartment was, however, only mildly impacted at 1-year of age (**SUP TABLE4**) suggesting that the first changes in immune cell populations target mainly the spleen.

Perturbation of XCI is associated with additional signs of autoimmunity in aging mice

Mo/MΦ and dendritic cell expansion are typical of inflammation reported in mouse models of SLE including NZB/W F1 and Yaa mice in which *Tlr7* is overexpressed[12,18]. This prompted us to investigate other known signs of autoimmunity. Accordingly, we observed higher percentages of spontaneously activated B and T cells in the spleen of 1-year-old *Ftx* KO

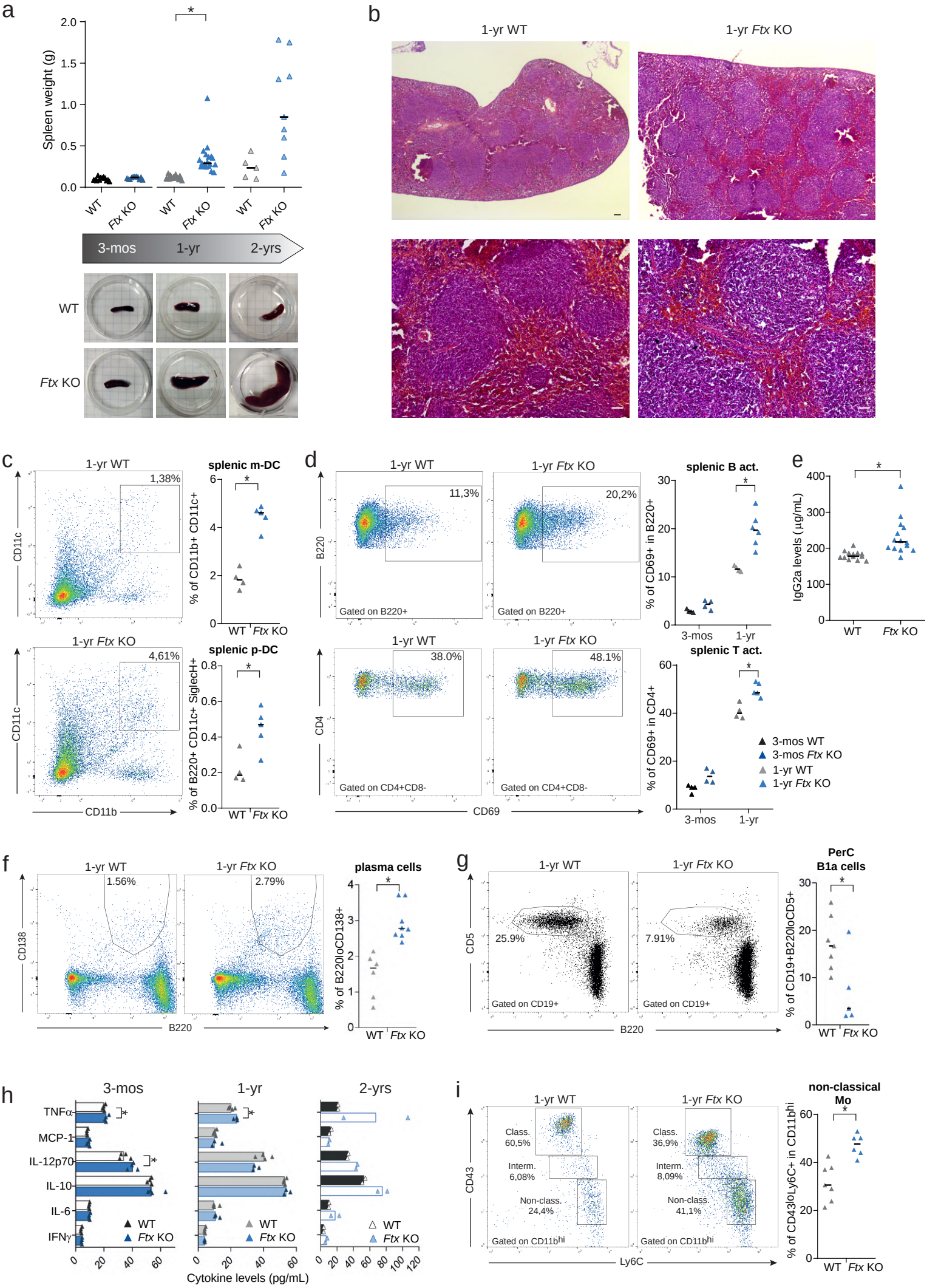
a
Spleen weight (g)
2.0
1.5
1.0
0.5
0.0
*
WT
Ftx KO
WT
Ftx KO
WT
Ftx KO
3-mos
1-yr
2-yrs
WT
Ftx KO
b
1-yr WT
1-yr Ftx KO
c
1-yr WT
1,38%
CD11c
splenic m-DC
% of CD11b+ CD11c+
WT
Ftx KO
1-yr Ftx KO
4,61%
CD11b
splenic p-DC
% of B220+ CD11c+ SiglecH+
d
1-yr WT
11,3%
B220
Gated on B220+
1-yr Ftx KO
20,2%
Gated on B220+
splenic B act.
% of CD69+ in B220+
3-mos
1-yr
1-yr WT
38.0%
CD4
Gated on CD4+CD8-
1-yr Ftx KO
48.1%
Gated on CD4+CD8-
CD69
splenic T act.
% of CD69+ in CD4+
3-mos WT
3-mos Ftx KO
1-yr WT
1-yr Ftx KO
e
IgG2a levels (µg/mL)
WT
Ftx KO
f
1-yr WT
1.56%
CD138
B220
1-yr Ftx KO
2.79%
plasma cells
% of B220loCD138+
g
1-yr WT
25.9%
CD5
Gated on CD19+
B220
1-yr Ftx KO
7.91%
Gated on CD19+
PerC B1a cells
% of CD19+B220loCD5+
h
3-mos
1-yr
2-yrs
TNFα
MCP-1
IL-12p70
IL-10
IL-6
IFNγ
WT
Ftx KO
Cytokine levels (pg/mL)
i
1-yr WT
CD43
Class. 60,5%
Interm. 6,08%
Non-class. 24,4%
Gated on CD11bhi
Ly6C
1-yr Ftx KO
Class. 36,9%
Interm. 8,09%
Non-class. 41,1%
Gated on CD11bhi
non-classical Mo
% of CD43loLy6C+ in CD11bhi

Figure 2

Figure 2. *Ftx* KO females show signs of virgin inflammation and autoimmune manifestations at 1-year of age.

- **a.** Spleen weight of wild-type (WT) and *Ftx* KO females at 3-months, 1-year and 2-years of age. Median values are shown. (*t-test*, **p*-values < 0.05). Underneath, representative images of WT and *Ftx* KO spleens from 3-month, 1-year and 2-year-old females.
- **b.** Representative images of hematoxylin-eosin staining on sections of spleens from 1-year-old WT and *Ftx* KO females. Scale bar; 100 μm.
- **c.** Representative flow cytometry analysis of splenic myeloid dendritic cells (m-DC) in WT and *Ftx* KO 1-year-old females. On the right, percentages of splenic m-DC ($CD11b^{+}CD11c^{+}$) and splenic plasmacytoid dendritic cells (p-DC) ($CD11c^{+}B220^{+}SiglecH^{+}$) in leucocytes. Each triangle represents a mouse. Median values are shown. (*t-test*, **p*-values < 0.05).
- **d.** Representative flow cytometry analysis of spontaneously activated B cells ($B220^{+}CD69^{+}$) (upper panels) or of spontaneously activated T cells ($CD4^{+}CD69^{+}$) (lower panels) in spleen from 1-year-old WT and *Ftx* KO females. Percentages in leucocytes are shown on the graphs beneath. Each triangle represents a mouse. Median values are shown. (*t-test*, **p*-values < 0.05).
- **e.** IgG2a natural antibody levels in sera of 1-year- and 2-year-old WT or *Ftx* KO females measured by ELISA. Each triangle represents a mouse. Median values are shown. (*t-test*, **p*-values < 0.05).
- **f.** Representative flow cytometry analysis of ($B220^{+}CD138^{+}$) plasma cells in the spleen of 1-year-old WT and *Ftx* KO females. Percentages in leucocytes are shown on the graphs beneath. Each triangle represents a mouse. Median values are shown. (*t-test*, **p*-values < 0.05).
- **g.** Representative flow cytometry analysis of ($CD19^{+}B220^{lo}CD5^{+}$) natural antibody producing B1a in the peritoneal cavity (PerC) of 1-year-old WT and *Ftx* KO females. Percentages in leucocytes are shown on the graphs beneath. Each triangle represents a mouse. Median values are shown. (*t-test*, **p*-values < 0.05).
- **h.** Cytokines levels in the blood analysed with CBA assays on sera from 3-month-, 1-year-, or 2-year-old WT and *Ftx* KO females. Each triangle represents a mouse. Median values are shown. (*t-test*, **p*-values < 0.05).
- **i.** Representative flow cytometry analysis of monocyte populations including non-classical ($CD11b^{hi}CD43^{lo}Ly6C^{+}$) scavenger monocytes in the spleen of 1-year-old WT and *Ftx* KO females. Percentages in leucocytes are shown on the graphs beneath. Each triangle represents a mouse. Median values are shown. (*t-test*, **p*-values < 0.05).

Table 1. Splenic cell distribution in WT and *Ftx* $^{-/-}$ female mice.

Values denote percentages (mean ± SD) of splenic nucleated cells except for erythroid cells where they stand for the percentage of splenic cells. n ≥ 4, t-test versus WT, *p < 0.05; § p <0.01, N.D. not determined.

	3-mos		1-yr	
	WT	*Ftx* KO	WT	*Ftx* KO
B cells ($CD19^+$)	50.7 ± 3.5	54.2 ± 6.4	48.0 ± 5.0	34.0 ± 3.0 *
MZ B cells ($CD19^+B220^+CD21^+CD23^-$)	3.7 ± 0.9	3.4 ± 1.1	5.1 ± 0.9	3.5 ± 2.3
Follicular B cells ($CD19^+B220^+CD21^{int}CD23^+$)	32.5 ± 2.6	33.3 ± 6.9	31.6 ± 4.8	20.7 ± 6.1 §
Transitional B cells ($CD19^+B220^+CD21^{lo}CD23^-IgM^+$)	3.6 ± 0.7	3.6 ± 0.9	5.5 ± 1.9	4.3 ± 1.3
T cells ($CD3^+$)	33.9 ± 2.6	31.0 ± 3.5	21.5 ± 5.4	23.1 ± 3.9
Cytotoxic T ($CD8^+CD4^-$)	11.2 ± 1.8	12.3 ± 2.1	20.3 ± 0.8	22.2 ± 5.0
Helper T ($CD8^-CD4^+$)	16.9 ± 0.9	18.5 ± 2.9	11.0 ± 0.8	16.3 ± 1.4 §
Myeloid ($CD11b^+$)	4.8 ± 1.4	4.4 ± 0.9	8.7 ± 2.5	15.3 ± 3.3 *
Mo/MΦ ($CD11b^+F4/80^+$)	2.2 ± 0.5	1.6 ± 0.2	3.7 ± 0.8	7.8 ± 2.6 *
Dendritic ($CD11c^+$)	2.7 ± 0.2	3.1 ± 0.7	4.0 ± 0.5	8.6 ± 1.3 §
m-DC ($CD11c^+CD11b^+$)	1.3 ± 0.1	1.5 ± 0.4	1.8 ± 0.4	4.4 ± 0.5 §
p-DC ($CD11c^+B220^+SiglecH^+$)	0.27 ± 0.1	0.22 ± 0.08	0.22 ± 0.09	0.45 ± 0.18 *
Erythroid cells ($Ter119^+$)	48.0 ± 4.3	47.3 ± 8.5	49.4 ± 4.4	55.8 ± 6.2
Cell count (x 10^6)	155 ± 10	173 ± 13	156 ± 39	384 ± 67 *

females compared to WT (**Fig. 2d**). Another classical manifestation of autoimmunity is the overproduction of natural antibodies. We therefore measured IgG2a levels – an auto-antibody abundant in *Tlr7*-driven autoimmune conditions[12,31] – in sera of 1-year-old KO vs WT females by ELISA and observed significantly higher levels in KO animals (**Fig. 2e**). In agreement, percentages of antibody-producing cells were increased for B220^{lo}CD138^{+} plasma cells in the spleen (**Fig. 2f**) and reduced for B1a cells in the peritoneal cavity (PerC) in 1-year-old *Ftx* KO females compared to WT females (**Fig. 2g**). This mimics the situation in systemic autoimmunity triggered by *Tlr7* overexpression in which B1a cells desert the PerC to migrate to the splenic compartment[31]. These changes were however not associated with any drastic increase in cytokine levels in the serum of 3-month- or 1-year-old *Ftx* KO females (**Fig. 2h**). Only a mild increase of *TNFα* levels – one of the cytokines induced by *TLR7* signalling – appeared consistently detected at 3-months and 1-year of age suggesting that cytokine levels are efficiently controlled despite the signs of inflammation which probably contributes to attenuate the phenotype that is observed at these ages. In contrast, we detected higher levels of *TNFα*, *IL-12p70*, *IL10* and *IL6* in sera of 2-year-old *Ftx* KO females compared to WT suggesting that compensatory mechanisms at play in young mice may deteriorate with aging (**Fig. 2h**).

Given that the effect of *Xist* perturbation on X-linked expression is especially pronounced in Mo/MΦ, we examined the populations of circulating Mo/MΦ in 1-yr females. We detected an over-representation of non-classical scavenger monocytes in the blood of *Ftx* KO females – a monocyte population recruited at inflammatory tissues in autoimmune contexts (**Fig. 2i**), but we did not observe signs of inflammation in peripheral tissues like kidneys, a clinical manifestation that is observed at late stages of SLE (data not shown).

Thus, *Ftx* KO females progressively develop a splenomegaly during aging which is characterised by a multilineage expansion. Splenic defects are accompanied by multiple signs of autoimmunity including high level of spontaneous lymphocyte activation and overproduction of IgG2a autoantibodies and by exacerbated differentiation of monocytes into scavenger subtypes.

<u>Inefficient negative feed-back of *TLR7* pathway upon perturbation of XCI in macrophages</u>

Ftx KO females develop a rather mild autoimmune phenotype compared to other mouse models in which *TLR7* pathway is overactive[12,31]. This may either relate to the fact that *Xist* perturbation only results in a ~2-fold increase in *Tlr7* RNA levels or be due to overexpression of other genes like *Tlr8* that counteract *TLR7* increase[31]. To test whether *TLR7* pathway overactivity could be one of the drivers of *Ftx* KO inflammatory phenotype and identify the targeted cell populations, we first measured the basal expression of cytokine genes normally

induced upon activation of *TLR7* pathway (ie. *Tnfα*, *Il1β*, *Il-6* and *Il-10*) by RT-qPCR in BM or splenic Mo/MΦ, in splenic DC and in splenic B cells of 1-year-old females (**Fig. 3a**). Basal RNA levels of *Il-10*/*Il1β* and *Tnfα* appeared significantly higher in Mo/MΦ and/or in splenic B cells of *Ftx* KO mice respectively, *Il6* showed tendencies to be overexpressed in splenic Mo/MΦ and B cells while *Tgfβ1* – a gene that is not a direct target of the *TLR7* pathway – was expressed at the same levels in WT and *Ftx* KO contexts (**Fig. 3a**). This modest induction of the pathway in 1-year-old KO females in absence of stimulation translates only mildly on circulating cytokines (**Fig. 2h**) suggesting that post-transcriptional regulations of cytokine levels may be operating in these animals. Of note, given the *IL-10* anti-inflammatory function, induction of *Il-10* transcription in *Ftx* KO females may also result from secondary response to inflammation signs and resembles tolerance phenomena that occur during chronic inflammation.

We then compared the responsiveness of *TLR7* pathway upon stimulation of *Ftx* KO vs WT immune cells through *in vitro* activation with agonists specific for ligands of *TLR7/8* (CL097), of *TLR4* (LPS) or of *TLR9* (CpG) on splenic B cells, BM-derived MΦ and DC from 1-year-old females[31]. No difference in early induction of target cytokines (*TNFα*, *IL1β* and *IL-6*) as measured by RT-qPCR could be detected between KO and WT cells. Instead, we observed a significant delay in the restoration of cytokine RNA levels upon *TLR7/8* stimulation specifically (**Fig. 3b**). This inefficient negative feed-back leads to drastically increased levels of cytokine mRNAs upon 8 hours of induction in *Ftx* KO MΦ (**Fig. 3b**). This effect was only detected in MΦ and not in B cells or DC (**SUP5**).

We conclude that *Ftx* KO Mo/MΦ are unable to efficiently repress *TLR7/TLR8* pathway upon activation. This may participate in creating an over-reactive immune environment that progressively become inflammatory.

Discussion

With recent world-wide waves of viral infections and increased realisation that women are significantly more resistant to these infections than men, understanding the basis of sexual dimorphism in immune system competence has emerged as critical to the design of new therapeutic strategies[35]. In this framework, we show here that perturbing the regulation of X-chromosome inactivation – a female-specific epigenetic process that is established early during development – directly impacts female immune response in mouse adult life. More specifically, certain X-linked genes with immune functions that naturally show a tendency to escape from XCI are expressed from the inactive X in higher percentages of immune cells upon XCI perturbation, resulting in overall higher levels of expression. This deregulation is associated with the progressive development of autoimmune manifestations indicative of an

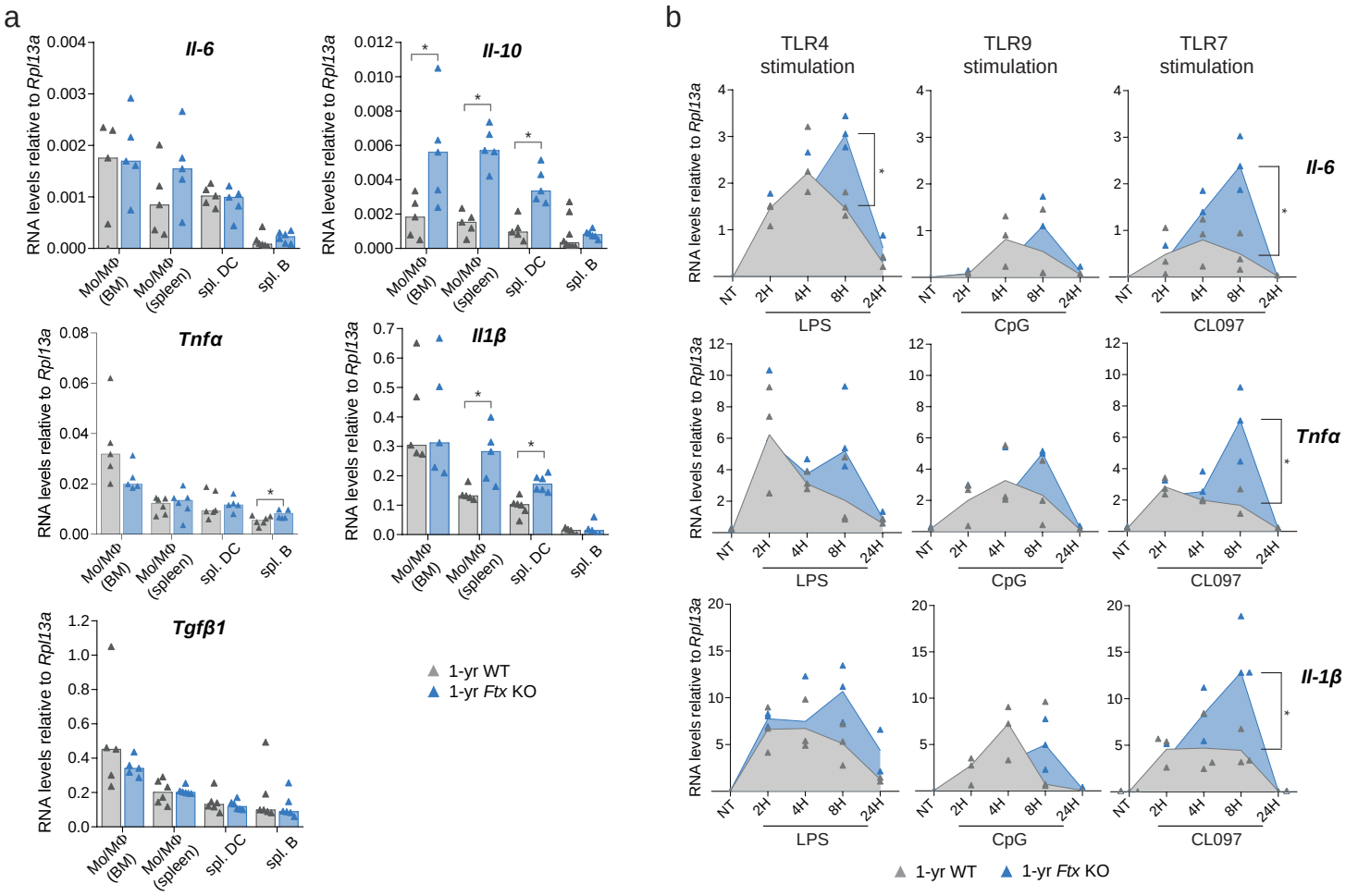
a
Il-6
Il-10
Tnfα
Il1β
Tgfβ1
RNA levels relative to Rpl13a
Mo/Mφ (BM)
Mo/Mφ (spleen)
spl. DC
spl. B
1-yr WT
1-yr Ftx KO
b
TLR4 stimulation
TLR9 stimulation
TLR7 stimulation
NT
2H
4H
8H
24H
LPS
CpG
CL097
Il-6
Tnfα
Il-1β
1-yr WT
1-yr Ftx KO

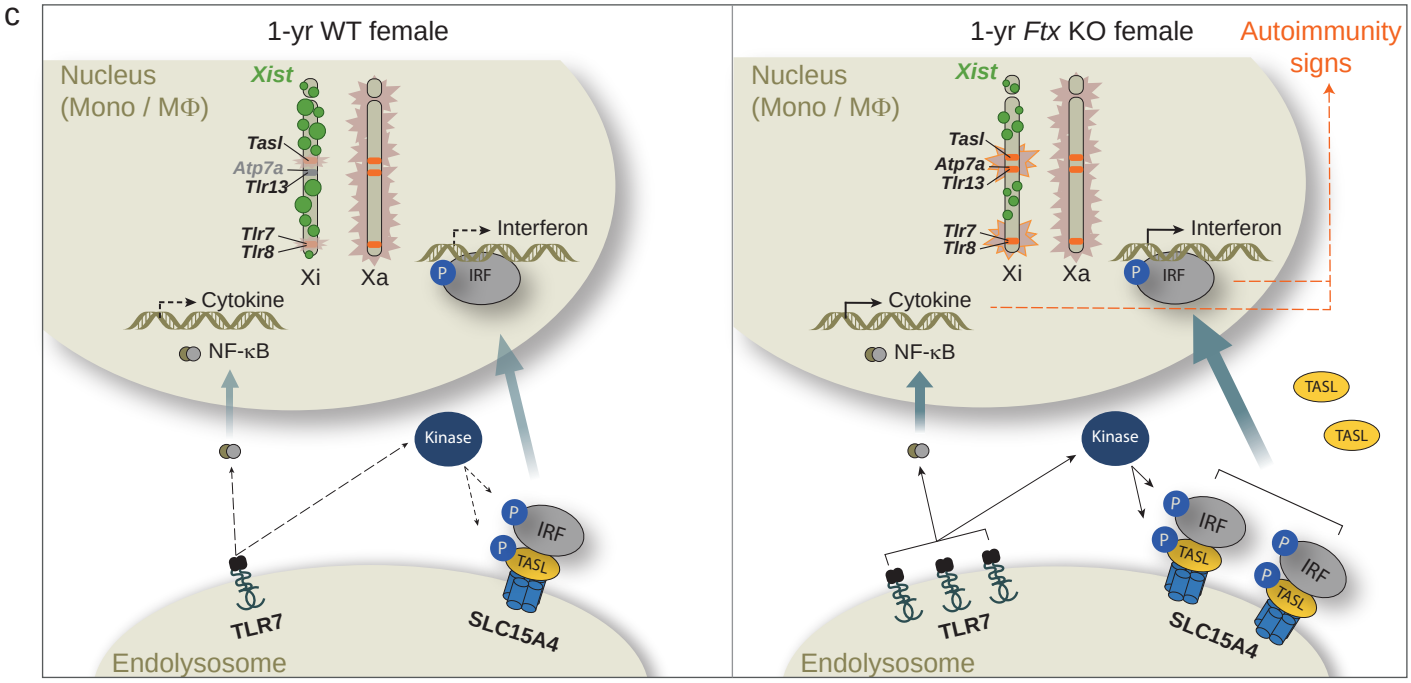
c
1-yr WT female
1-yr Ftx KO female
Autoimmunity signs
Nucleus (Mono / MΦ)
Xist
Tasl
Atp7a
Tlr13
Tlr7
Tlr8
Xi
Xa
Interferon
Cytokine
NF-κB
IRF
P
Kinase
TASL
TLR7
SLC15A4
Endolysosome

Figure 3

Figure 3. Deficient negative feedback of *TLR7* pathway in 1-year-old *Ftx* KO females.

a. Analysis of cytokine RNA levels by RT-qPCR in the indicated cell population collected from WT or *Ftx* KO 1-year-old females. Each triangle represents a mouse. Bar plots show median values. (*t-test*, **p*-values < 0.05).

b. RT-qPCR analysis of cytokine RNA levels in BM-derived macrophages (GM-CSF differentiation of total BM cells) activated either with LPS (*TLR4* pathway), CpG (*TLR9* pathway) or with the *TLR7* agonist CL097. Cells were either not treated (NT) or treated for 2, 4, 8 or 24 hours. Each triangle represents a mouse. Median values are shown. (*t-test*, **p*-values < 0.05).

c. A scenario of molecular events linking alteration of X-inactivation to mild autoimmune signs in 1-year *Ftx* KO females. In WT Mo/MΦ of 1-year-old females, *Xist* RNA accumulation on the inactive X-chromosome is reduced (as compared to other non-immune cell types) and silencing of specific loci – including *Tlr7* – is relaxed allowing for transcription of the corresponding genes at a low level. In the absence of stimulation of immune cells, this extra transcription from the Xi does not trigger any immune response. In *Ftx* KO Mo/MΦ of 1-year-old females, *Xist* RNA localization to the Xi is either absent or dramatically reduced, transcription of genes with a tendency to escape from XCI (i.e. *Tlr7*) is exacerbated and additional genes of the Xi (*Tlr13, Tasl*) are reactivated. This notably leads to higher number of *TLR7* receptors at the lysosome membrane, higher concentration of *TASL* in the cytoplasm and low-level ectopic activation of cytokine transcription and production. This ultimately promotes mild signs of inflammation.

over-reactive immune system. This suggests that, under normal conditions, low-level of escape from XCI of specific X-linked genes leads to a slightly higher dosage of the corresponding immune factors compared to males which may endow females with enhanced plasticity in immune responses. This hypothesis is corroborated by former observations that correlate higher expression of some X-linked genes (*Tlr7*, *Cxcr3*) in females compared to males with better protection against viral or parasite infections in both humans and mice[36,37]. Moreover, a recent study has identified loss-of-function mutations of TLR7 associated with severe forms of COVID-19 in young men, suggesting a key role of TLR7 pathway in the protective response against SARS-CoV2[38]. Some genes impacted by XCI perturbation in our study have also been associated with systemic autoimmune disorders in human: a *TLR7* gain-of-function mutation is associated with lupus development in human[13] while a SNP located 3' of *TASL* is associated with SLE susceptibility[33].

Different X-linked genes appear overexpressed upon XCI alteration depending on immune cell types (ie, *Cxcr3* in T cells, *Tlr7* in B cells, *Tlr7*, *Cybb* and *Tlr8*, in splenic DCs, *Tlr7*, *Tlr8*, *Tlr13*, *Tasl*, *Il2rg* and *Atp7a* in monocyte/macrophages) suggesting that various molecular pathways are affected in immune cells. The number of affected genes might be underestimated since we tested a subset of immune-related X-linked genes. Therefore, the phenotype we observe probably results from the combination of effects ensuing from distinct reactivation events in different cell types. We focussed on the consequences of *Tlr7* overexpression in our system, one of the few genes with higher expression in multiple immune cell types. We found that biallelic expression of *Tlr7* and of *Tasl* – a gene acting downstream in the *TLR7* signalling pathway[39] – occurs more frequently upon XCI perturbation in monocytes/macrophages. This suggests a scenario whereby a higher number of these two factors at the lysosome membrane and in the cytoplasm respectively, leads to up-regulation of target genes (cytokine and interferons), which participates in promoting weak signs of infection (**Fig. 3c**). Intriguingly, both *Tlr7* and *Tlr8*, two genes with opposite roles in the development of autoimmunity appear overexpressed in monocytes/macrophages. The formation of *TLR8/TLR7* heterodimers at the lysosome membrane has been proposed to exert a neutralising effect on *TLR7* pathway activation[31]. This is likely to occur in *Ftx* KO monocytes/macrophages and may participate in the weakening of autoimmune signs.

What is the molecular mechanism underlying reactivation of specific X-linked genes in *Ftx* KO females? Intriguingly, we noticed that genes sensitive to *Xist* perturbation tended either to cluster on the X-chromosome (*Tlr7/Tlr8* and *Atp7a/Tlr13*) or to be located in gene-poor regions (*Cxcr3*, *Cybb*) (**Fig. 1c**), suggesting a mechanism that operates regionally over several kilobases rather than an action restricted to promoters. In this regard, silencing of *TLR7* and, more generally, of X-linked genes lacking promoter DNA methylation in human B cells, is

thought to depend on continuous association with *XIST* RNA and *XIST*-dependent H3K27 deacetylation of distal enhancers and not promoters[19]. In female mouse monocyte/macrophages, the methylation status of the promoter of genes targeted by reactivation is unknown but it is conceivable that, in the *Ftx* KO context, reduced deacetylation of local enhancers following *Xist* RNA delocalisation from the Xi, facilitated by reduced accumulation of histone repressive marks[15], contributes to enhance reactivation of neighbouring genes. Another intriguing observation is the inefficient negative feed-back of cytokine gene expression upon *TLR7* activation. Whether this is to relate to impaired re-localisation of *Xist* RNA to the Xi upon stimulation and, therefore, to sub-efficient secondary repression of *Tlr7* Xi copy remains to be addressed. Finally, it is tempting to postulate the existence of an active process that would have been evolutionary selected to maintain low-levels of XCI escape of specific X-linked genes since this may both confer a greater resistance to infection to female individuals and prevent autoimmunity.

Molecular and cellular phenotypes resulting from impaired *Xist* expression progress gradually with age. Even though we cannot exclude that *Xist* expression depends on *Ftx* in immune cells specifically, it is more likely that XCI perturbation in *Ftx* KO females initiates in the embryo and is transmitted, as such, to the hematopoietic lineage. This perturbation has, however, almost no detectable effect in immune cells from 3-month-old females and does not really affect life expectancy or animal fitness with age. Of note, in this study, animals have been kept in a pathogen-free environment; we cannot therefore exclude that exogenous aggressions of *Ftx* KO immune system would result in stronger phenotypic manifestations. This lack of marked phenotype suggests that compensatory adjustments are at work in young females, which may not be surprising since immune cells and the whole immune compartment are intrinsically built to respond and adapt. However, from 1-year of age onwards, silencing of specific genes on the Xi and the balance between immune cell populations are progressively lost. Whether this collapse relates to changes in heterochromatin features that are known to occur during aging[40] and/or whether it is accelerated by the gradual loss of immune cell differentiation potential[41] remains to be determined. In this regard, it is tempting to speculate that deregulation of XCI may also contribute to autoimmune conditions that appear in young girls or to autoimmune phenotypes specific to postmenopausal women (rheumatoid arthritis[42], some forms of Sjögren's syndrome[43], atherosclerosis or of ischemic heart diseases[35,44], inflammaging[45]) when estrogen levels are low and cannot account for the sexual dimorphism observed in these diseases. In conclusion, we have established a direct link between XCI maintenance and function of the immune system. This suggests further studies to explore the role of XCI regulators in unexplained forms of autoimmune conditions either in young children or in elder women and opens up new potentials for therapeutic strategies.

Methods

Generation of *Ftx* deficient mice

Ftx-deficient mice were generated in the Institut Clinique de la Souris (Illkirch, France). The strategy used to create *Ftx* KO mice on a C57BL/6N background is depicted in **SUP6**. *Ftx* KO females were generated either by mating $Ftx^{-/Y}$ males with $Ftx^{+/-}$ heterozygote females or by mating $Ftx^{-/Y}$ males with $Ftx^{-/-}$ KO females. Similar results were obtained on females $Ftx^{-/-}$ KO mice from either cross. Mice were maintained under specific pathogen-free conditions in the animal facility of the Jacques Monod Institute (Paris, France) and handled following the European Community guidelines (project authorization # 05353.02 approved by the ethical comity of the French Ministry for Scientific Research). Virgin females with no signs of inflammation from self-inflicted or other injuries have been used exclusively.

Flow cytometry analyses

Bone marrow, spleen, blood and peritoneal cavity cells were stained using the following antibodies: CD3 PerCP-Vio770 (130-119-656, Miltenyi Biotec), CD4- APC (130-123-207, Miltenyi Biotec), CD5-APC-Vio770 (130-120-165, Miltenyi Biotec), CD8-FITC (130-118-468, Miltenyi Biotec), CD11b APC (553312, BD Pharmingen), CD11c PE-Vio770 (130-110-840, Miltenyi Biotec) , CD19-FITC (557398, BD Pharmingen), CD21-APC-Vio770 (130-111-733, Miltenyi Biotec), CD23-PE-Vio770 (130-118-764, Miltenyi Biotec), CD38-PE (130-123-571, Miltenyi Biotec) , CD43-PE (130-112-887, Miltenyi Biotec), CD69-PE (130-115-575, Miltenyi Biotec), CD138 PE-Vio615 (130-108-989, Miltenyi Biotec), F4/80 FITC (130-117-509, Miltenyi Biotec), Ter119 PE (130-112-909, Miltenyi Biotec), SiglecH APC-Vio770 (130-112-299, Miltenyi Biotec), B220-APC (130-110-847, Miltenyi Biotec), B220 VioBlue (130-110-851, Miltenyi Biotec), IgM-VioBlue (130-116-318, Miltenyi Biotec), IgD-PE (130-111-496, Miltenyi Biotec), GL7-PE-Cy7 (144619, BioLegend), Ly6C-FITC (130-111-915, Miltenyi Biotec) following recommendations of the manufacturers. Flow cytometry was conducted on a BD FACSAria Fusion (BD Biosciences) at the Imagoseine platform of the Jacques Monod Institute (Paris, France). The instrument is equipped with 18 detectors and 5 lasers (UV 355nm 20mW, Violet 405nm 10 mW, Blue 488nm 13mW, Yellow-Green 561nm 50mW, and Red 633nm 11mW). The Cytometer Setup and Tracking (CS&T) RUO beads (Lot ID 82169) were used to establish reference fluorescence intensities for measuring instrument sensitivity over time. At least 50 000 single cells were acquired. Data files were exported to FCS file 3.1. All manual analysis was performed using FlowJo 10.8.1 (BD Biosciences). Signal stability over time was checked using flowClean plugin. FSC height (FSC-H) and area (FSC-A) are plotted against each other and used to eliminate doublets and aggregates.

RT-qPCR analyses

Total RNA from specific cell populations collected by FACS was isolated using RNeasy MinElute kit (Qiagen) following manufacturer recommendations. RNA from a minimum of 50 000 cells was reversed transcribed with Superscript IV reverse transcriptase (18090200, ThermoFisher Scientific) and random hexamers (Promega) as primers according to manufacturer's recommendations. Control reactions lacking enzyme were systematically run in parallel as negative controls. 10 μl real-time quantitative PCR were performed on 1μl of diluted RT reactions (1/5) using Power SYBR green PCR Master mix (4368708, ThermoFisher Scientific) on Viia7 qPCR machine (ThermoFisher Scientific). All samples were run in duplicates. Expression levels were normalized to the reference gene *Rpl13a*. For primer sequences see **SUP TABLE 5**.

RNA-FISH

Cell preparation. FACS sorted cells were allowed to sediment on poly-lysine coated slides (ThermoFisher Scientific) in a 50 μl drop of PBS1X for 15 minutes at room temperature, fixed for 10 min in an ice-cold 3% paraformaldehyde/PBS1X solution (Electron Microscopy Science) and permeabilized for 5-10 min in ice-cold CSK buffer (10mM 30 PIPES; 300mM sucrose; 100mM NaCl; 3mM MgCl2; pH6.8) supplemented with 0.5% Triton X-100 (Sigma-Aldrich) and 2mM Vanadyl-ribonucleoside-complex (New England Biolabs).

Probe preparation. 1µg of purified fosmid/BAC DNA purified using standard alkaline lysis protocol was labelled with fluorescent dUTPs (SpectrumOrange and SpectrumGreen from Abott Molecular and Cy5-UTPs from GE HealthCare Life Science) in a 50μl nick-translation reaction for 3h at 15°C.

Xist: p510 plasmid[46]; *Ftx*: fosmid probe (WI1-1177B13, BACPAC); *Tlr7*: fosmid probes (WI1-1548K9, WI1-977A7, BACPAC); *Tasl*: fosmid probes (WI1-1708P12, WI1-841O8, BACPAC)

Hybridization. 100 ng of probe were co-precipitated with 3µg of *Cot-I* DNA (Invitrogen) and 10µg of Sheared Salmon Sperm DNA (Invitrogen) using 1/10 3M NaOAc and 2.5 volumes of ethanol for 3 hours at -20°C. Precipitated probes were washed with 70% ethanol and resuspended in formamide (deionized formamide > 99.5%, Sigma Aldrich), then denatured for 7 min at 75°C. After probe denaturation, an equivalent volume of 2X hybridization buffer (4X saline sodium citrate (SSC, Ambion), 20% dextran sulfate, 2mg/ml BSA (New England Biolabs), and 2mM Vanadyl Ribonucleoside Complex (VRC, New England Biolabs)) was added, and slides were hybridized overnight at 37°C in a humid chamber. The slides were subsequently washed three times in 50% formamide/2X SSC [pH 7.2] at 42°C for 5 min each, and three times in 2XSSC at 42°C for 5 min each. Slides were mounted in Vectashield containing DAPI (Vector Laboratories).

Microscopy and image analysis.

Images were taken on an Axioplan 2 Imaging fluorescence microscope (Zeiss) with a cooled Coolsnap camera (Roper Scientifics) or a DMI-6000 inverted fluorescence microscope with a motorized stage (Leica) and a CCD Camera HQ2 (Roper Scientific), both controlled by the MetaMorph 7.04 software (Roper Scientifics), using a Plan-NEOFLUAR 63X/1.25 oil objective (Zeiss), a Plan-NEOFLUAR 100X/1.30 oil objective (Zeiss), or a HCX PL APO 63X/1.4 oil objective (Leica). Optical sections were collected at 0.2 mm steps through each nucleus at different wavelengths (nm) (Zeiss: DAPI [345,455], FITC [488,507], CY3 [(625)650,670]) (Leica: DAPI [360,470], FITC [470,525] CY3 [550,570]). Approximately 40 optical sections per nucleus were collected. Stacks were processed using Icy (http://icy.bioimageanalysis.org), and the images are represented as 2D projections of the stacks (maximum projection).

Serological analyses

For IgG2a antibodies detection, we used the IgG2a Mouse uncoated ELISA kit (88-50420, ThermoFisher Scientific). Sera plates were precoated with anti-mouse IgG2a overnight and sera were applied at a 1:30 000 dilution. The assay was developed with HRP-labelled goat anti-mouse IgG antibody (ThermoFisher Scientific). A standard curve was calculated with purified mouse IgG2a (ThermoFisher Scientific). Plates were read at 450nm on an AMR-100 microplate reader (Allsheng). Levels of inflammatory cytokines in sera were measured using a cytometric bead array (CBA) mouse inflammation kit (552364, BD Biosciences) according to the manufacturer's instructions.

Cell sorting and activation

Magnetic sorting. After isolation, spleen or bone marrow cells were stained for 30 min on ice with Anti-CD23 Magnetic Microbeads (130-098-784, Miltenyi Biotec) or Anti-F4/80 Magnetic Microbeads (130-110-443, Miltenyi Biotec) or Anti-CD11b Magnetic Microbeads (130-126-725, Miltenyi Biotec) or CD11c Magnetic Microbeads (130-108-338, Miltenyi Biotec) or Anti-CD90.2 Magnetic Microbeads (130-121-278, Miltenyi Biotec), Anti-CD19 Magnetic Microbeads (130-121-301, Miltenyi Biotec), washed with PBS1X 3% FBS and centrifuged at 300g for 10 min. Cells suspension was purified on LS column (130–042-401, Miltenyi Biotec). Purity of sorted cells was controlled by cytometry using corresponding antibodies.
For differentiation of bone marrow derived cells into macrophages (BMDM), total bone marrow cells were cultured with GM-CSF (100ng/ml, Miltenyi Biotec, 130-095-742) in complete RPMI 1640 (RPMI 1640 + Glutamax, 10% FBS, 1mM Sodium Pyurvate, 10mM Hepes, 0,1mM NEAA, 50µM βmercaptoethanol)

For differentiation of bone marrow derived cells into dendritic cells (BMDC), total bone marrow cells were cultured with GM-CSF (20ng/ml) in complete RPMI 1640. Differentiation efficiencies were checked by cytometry using a CD11c, CD11b, F4/80, CD3, B220 antibody panel.

Cell Activation. BMDM and BMDC were stimulated with: LPS (1ng/ml, Sigma-Aldrich) for TLR4 activation, CpG ODN 2395 (100nM; tlrl-2395, InvivoGen) for TLR9 activation or CL097 (50nM; tlrl-c97, InvivoGen) for TLR 7 activation.

Splenic B cells were stimulated with: LPS (1µg/ml, Sigma-Aldrich) for TLR4 activation, CpG ODN 2395 (1µM; tlrl-2395, InvivoGen) for TLR9 activation or CL097 (1µg/ml; tlrl-c97, InvivoGen) for TLR 7 activation. Matched negative controls ODN 5328 (InvivoGen) or CL075 (InvivoGen) were used for ODN 2395 and CL097 respectively.

Acknowledgments

We thank the Microscopy Platform-UMR7216 Epigenetic and Cell Fate center for access to instruments and technical advice. We acknowledge the ImagoSeine core facility of the Institut Jacques Monod, member of the France BioImaging infrastructure (ANR-10-INBS-04) and GIS-IBiSA and the support of La Ligue contre le Cancer (R03/75-79), in particular, we thank the Imagoseine cytometry platform, Souganya Many and Daniil Korenkov for technical assistance. We thank the cytometry platform of St Louis Hospital-INSERM UMRS 976. We thank the animal facility of the Jacques Monod Institute and Laetitia Pontoizeau in particular, for taking good care of the *Ftx* KO colony for such a long time. We thank Corinne Chureau for her help in the generation of *Ftx* KO mice. We thank Sophie Polo, Pierre-Antoine Defossez, Slimane Ait-Si-Ali and Jean-François Ouimette for critical reading of the manuscript. This study was supported by the ATIP/Avenir program (to C.R.) from the Centre National de la Recherche Scientifique (CNRS) and from the Institut National de la Santé et de la Recherche Medical (INSERM), by ERC starting grant #206875 (to C.R.), by the Agence Nationale de la Recherche (ANR) ANR-nonCodiX-14-CE10-0017-01 (to C.R.), by La Ligue nationale contre le cancer (to C.R.).

References

1. Klein, S. L. & Flanagan, K. L. Sex differences in immune responses. *Nat. Rev. Immunol.* **16**, 626–638 (2016).
2. Schurz, H. *et al.* The X chromosome and sex-specific effects in infectious disease susceptibility. *Hum. Genomics* **13**, 2 (2019).
3. Sauteraud, R. *et al.* Inferring genes that escape X-Chromosome inactivation reveals important contribution of variable escape genes to sex-biased diseases. *Genome Res.* (2021) doi:10.1101/gr.275677.121.
4. Sierra, I. & Anguera, M. C. Enjoy the silence: X-chromosome inactivation diversity in somatic cells. *Curr. Opin. Genet. Dev.* **55**, 26–31 (2019).
5. Credendino, S. C., Neumayer, C. & Cantone, I. Genetics and Epigenetics of Sex Bias: Insights from Human Cancer and Autoimmunity. *Trends Genet.* **36**, 650–663 (2020).
6. Yuen, G. J. Autoimmunity in women: an eXamination of eXisting models. *Clin. Immunol.* **210**, 108270 (2020).
7. Youness, A., Miquel, C.-H. & Guéry, J.-C. Escape from X Chromosome Inactivation and the Female Predominance in Autoimmune Diseases. *Int. J. Mol. Sci.* **22**, 1114 (2021).
8. Souyris, M. *et al.* TLR7 escapes X chromosome inactivation in immune cells. *Sci. Immunol.* **3**, eaap8855 (2018).
9. Antonelli, A. *et al.* Graves' disease: Epidemiology, genetic and environmental risk factors and viruses. *Best Pract. Res. Clin. Endocrinol. Metab.* **34**, 101387 (2020).
10. Souyris, M., Mejía, J. E., Chaumeil, J. & Guéry, J.-C. Female predisposition to TLR7-driven autoimmunity: gene dosage and the escape from X chromosome inactivation. *Semin. Immunopathol.* **41**, 153–164 (2019).
11. Bost, C. *et al.* Long non-coding RNA Xist contribution in systemic lupus erythematosus and rheumatoid arthritis. *Clin. Immunol.* **236**, 108937 (2022).
12. Deane, J. A. *et al.* Control of toll-like receptor 7 expression is essential to restrict autoimmunity and dendritic cell proliferation. *Immunity* **27**, 801–810 (2007).

13. Brown, G. J. *et al.* TLR7 gain-of-function genetic variation causes human lupus. *Nature* **605**, 349–356 (2022).
14. Loda, A., Collombet, S. & Heard, E. Gene regulation in time and space during X-chromosome inactivation. *Nat. Rev. Mol. Cell Biol.* **23**, 231–249 (2022).
15. Wang, J. *et al.* Unusual maintenance of X chromosome inactivation predisposes female lymphocytes for increased expression from the inactive X. *Proc. Natl. Acad. Sci. U. S. A.* **113**, E2029-2038 (2016).
16. Syrett, C. M. *et al.* Diversity of Epigenetic Features of the Inactive X-Chromosome in NK Cells, Dendritic Cells, and Macrophages. *Front. Immunol.* **9**, 3087 (2018).
17. Syrett, C. M., Sierra, I., Beethem, Z. T., Dubin, A. H. & Anguera, M. C. Loss of epigenetic modifications on the inactive X chromosome and sex-biased gene expression profiles in B cells from NZB/W F1 mice with lupus-like disease. *J. Autoimmun.* **107**, 102357 (2020).
18. Helyer, B. J. & Howie, J. B. Renal Disease associated with Positive Lupus Erythematosus Tests in a Crossbred Strain of Mice. *Nature* **197**, 197–197 (1963).
19. Yu, B. *et al.* B cell-specific XIST complex enforces X-inactivation and restrains atypical B cells. *Cell* **184**, 1790-1803.e17 (2021).
20. Yang, T., Ou, J. & Yildirim, E. Xist exerts gene-specific silencing during XCI maintenance and impacts lineage-specific cell differentiation and proliferation during hematopoiesis. *Nat. Commun.* **13**, 4464 (2022).
21. Yildirim, E. *et al.* Xist RNA is a potent suppressor of hematologic cancer in mice. *Cell* **152**, 727–742 (2013).
22. Yang, L., Kirby, J. E., Sunwoo, H. & Lee, J. T. Female mice lacking Xist RNA show partial dosage compensation and survive to term. *Genes Dev.* **30**, 1747–1760 (2016).
23. Yang, L., Yildirim, E., Kirby, J. E., Press, W. & Lee, J. T. Widespread organ tolerance to Xist loss and X reactivation except under chronic stress in the gut. *Proc. Natl. Acad. Sci. U. S. A.* **117**, 4262–4272 (2020).

24. Savarese, F., Flahndorfer, K., Jaenisch, R., Busslinger, M. & Wutz, A. Hematopoietic Precursor Cells Transiently Reestablish Permissiveness for X Inactivation. *Mol. Cell. Biol.* **26**, 7167–7177 (2006).
25. Chureau, C. *et al.* Ftx is a non-coding RNA which affects Xist expression and chromatin structure within the X-inactivation center region. *Hum. Mol. Genet.* **20**, 705–718 (2011).
26. Chureau, C. *et al.* Comparative Sequence Analysis of the X-Inactivation Center Region in Mouse, Human, and Bovine. *Genome Res.* **12**, 894–908 (2002).
27. Furlan, G. *et al.* The Ftx Noncoding Locus Controls X Chromosome Inactivation Independently of Its RNA Products. *Mol. Cell* **70**, 462-472.e8 (2018).
28. Hosoi, Y. *et al.* Female mice lacking Ftx lncRNA exhibit impaired X-chromosome inactivation and a microphthalmia-like phenotype. *Nat. Commun.* **9**, 3829 (2018).
29. Soma, M., Fujihara, Y., Okabe, M., Ishino, F. & Kobayashi, S. Ftx is dispensable for imprinted X-chromosome inactivation in preimplantation mouse embryos. *Sci. Rep.* **4**, 5181 (2014).
30. Forsyth, K. S. & Anguera, M. C. Time to get ill: the intersection of viral infections, sex, and the X chromosome. *Curr. Opin. Physiol.* **19**, 62–72 (2021).
31. Demaria, O. *et al.* TLR8 deficiency leads to autoimmunity in mice. *J. Clin. Invest.* **120**, 3651–3662 (2010).
32. Lacotte, S., Brun, S., Muller, S. & Dumortier, H. CXCR3, inflammation, and autoimmune diseases. *Ann. N. Y. Acad. Sci.* **1173**, 310–317 (2009).
33. Odhams, C. A. *et al.* Interferon inducible X-linked gene CXorf21 may contribute to sexual dimorphism in Systemic Lupus Erythematosus. *Nat. Commun.* **10**, 2164 (2019).
34. Duan, T., Du, Y., Xing, C., Wang, H. Y. & Wang, R.-F. Toll-Like Receptor Signaling and Its Role in Cell-Mediated Immunity. *Front. Immunol.* **13**, 812774 (2022).
35. Mauvais-Jarvis, F. *et al.* Sex and gender: modifiers of health, disease, and medicine. *Lancet Lond. Engl.* **396**, 565–582 (2020).

36. Fink, A. L., Engle, K., Ursin, R. L., Tang, W.-Y. & Klein, S. L. Biological sex affects vaccine efficacy and protection against influenza in mice. *Proc. Natl. Acad. Sci.* **115**, 12477–12482 (2018).
37. Oghumu, S. *et al.* Cutting Edge: CXCR3 Escapes X Chromosome Inactivation in T Cells during Infection: Potential Implications for Sex Differences in Immune Responses. *J. Immunol.* **203**, 789–794 (2019).
38. Asano, T. *et al.* X-linked recessive TLR7 deficiency in ~1% of men under 60 years old with life-threatening COVID-19. *Sci. Immunol.* **6**, eabl4348 (2021).
39. Heinz, L. X. *et al.* TASL is the SLC15A4-associated adaptor for IRF5 activation by TLR7-9. *Nature* **581**, 316–322 (2020).
40. Djeghloul, D. *et al.* Age-Associated Decrease of the Histone Methyltransferase SUV39H1 in HSC Perturbs Heterochromatin and B Lymphoid Differentiation. *Stem Cell Rep.* **6**, 970–984 (2016).
41. Denkinger, M. D., Leins, H., Schirmbeck, R., Florian, M. C. & Geiger, H. HSC Aging and Senescent Immune Remodeling. *Trends Immunol.* **36**, 815–824 (2015).
42. Krasselt, M. & Baerwald, C. Sex, Symptom Severity, and Quality of Life in Rheumatology. *Clin. Rev. Allergy Immunol.* **56**, 346–361 (2019).
43. Wang, Y. *et al.* TLR7 Signaling Drives the Development of Sjögren's Syndrome. *Front. Immunol.* **12**, 676010 (2021).
44. Björkegren, J. L. M. & Lusis, A. J. Atherosclerosis: Recent developments. *Cell* **185**, 1630–1645 (2022).
45. Márquez, E. J. *et al.* Sexual-dimorphism in human immune system aging. *Nat. Commun.* **11**, 751 (2020).
46. Debrand, E., Chureau, C., Arnaud, D., Avner, P. & Heard, E. Functional Analysis of the *DXPas34* Locus, a 3′ Regulator of *Xist* Expression. *Mol. Cell. Biol.* **19**, 8513–8525 (1999).

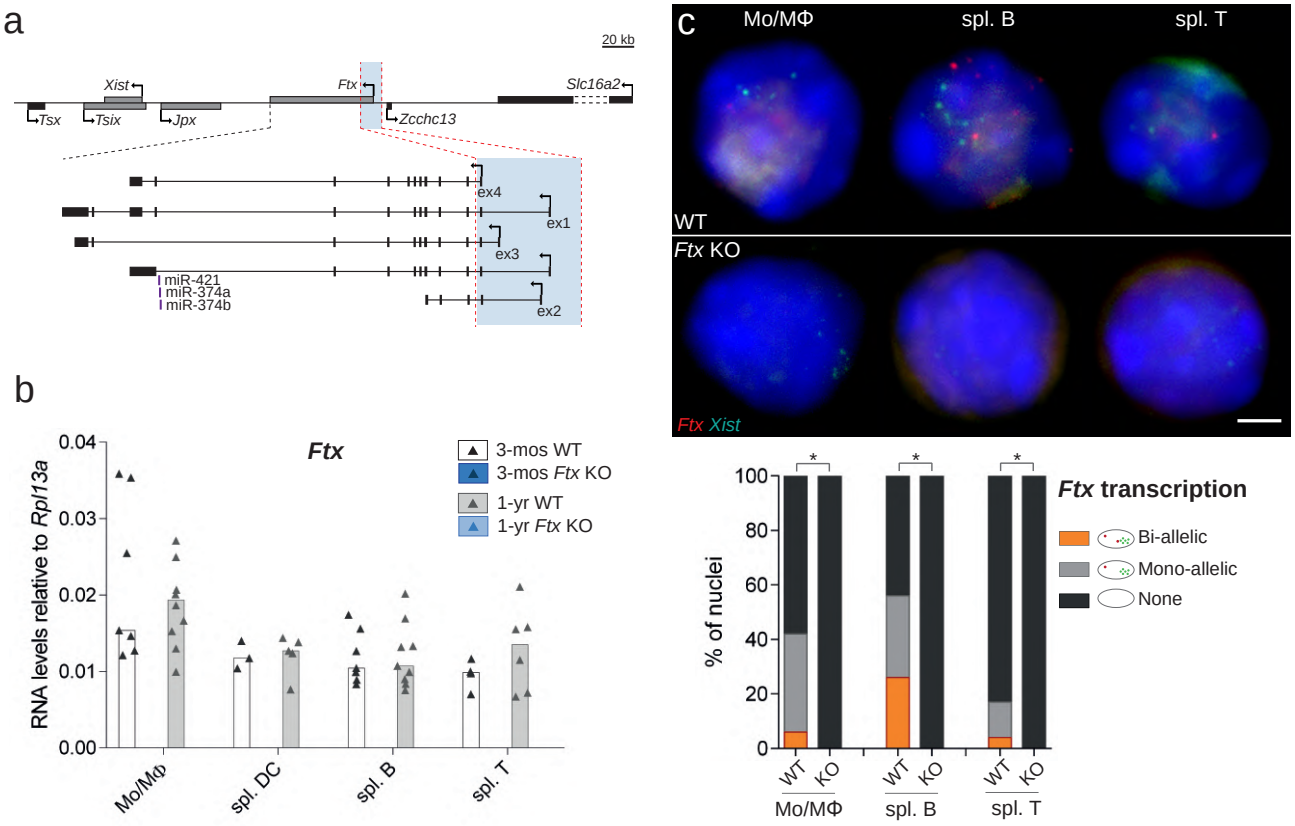
a
20 kb
Xist
Ftx
Slc16a2
Tsx
Tsix
Jpx
Zcchc13
ex4
ex1
ex3
ex2
miR-421
miR-374a
miR-374b
b
Ftx
RNA levels relative to Rpl13a
0.04
0.03
0.02
0.01
0.00
3-mos WT
3-mos Ftx KO
1-yr WT
1-yr Ftx KO
Mo/Mφ
spl. DC
spl. B
spl. T
c
Mo/MΦ
spl. B
spl. T
WT
Ftx KO
Ftx Xist
% of nuclei
100
80
60
40
20
0
Ftx transcription
Bi-allelic
Mono-allelic
None
WT
KO
Mo/MΦ
spl. B
spl. T

Sup 1

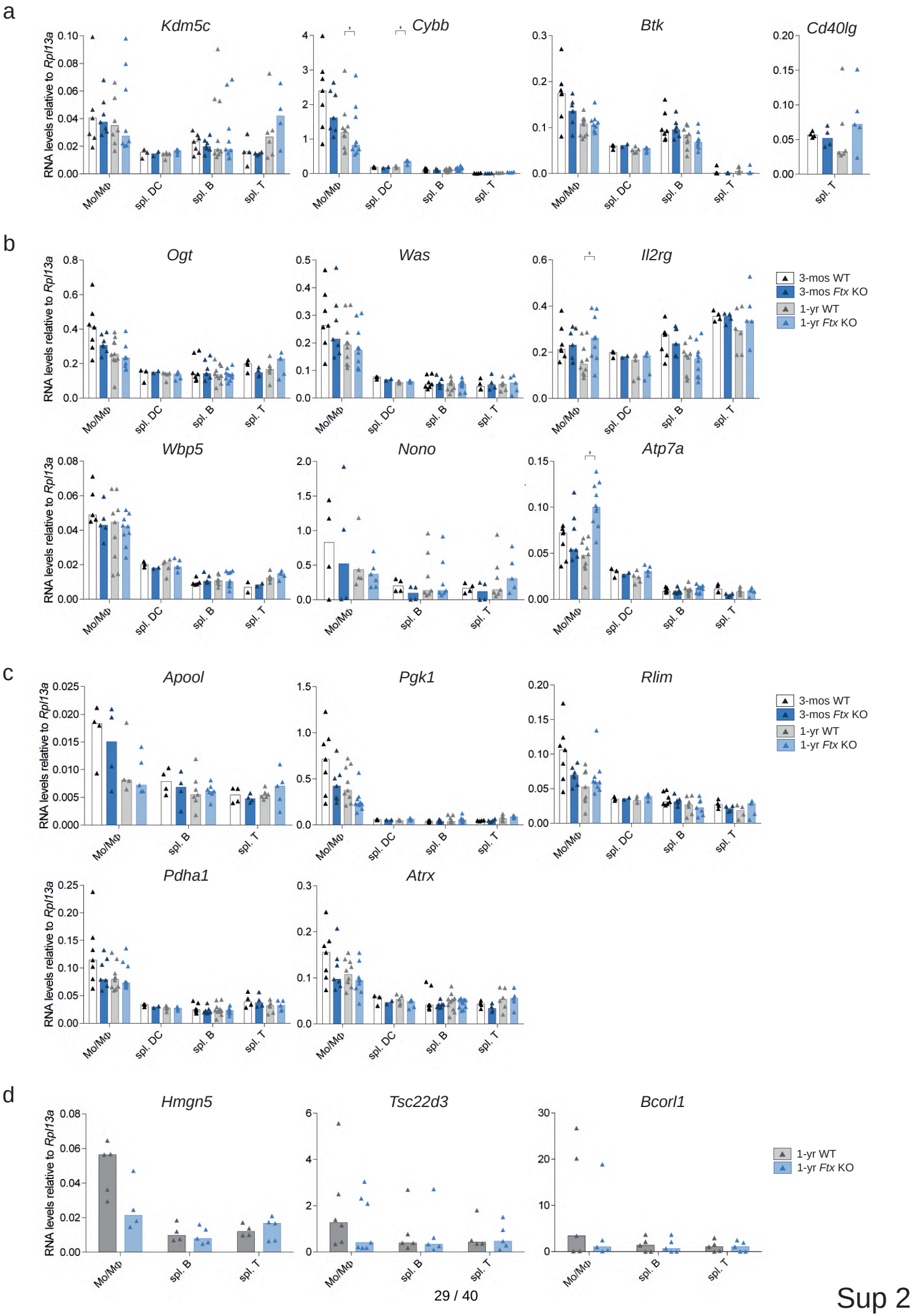
a
Kdm5c
Cybb
Btk
Cd40lg
b
Ogt
Was
Il2rg
Wbp5
Nono
Atp7a
c
Apool
Pgk1
Rlim
Pdha1
Atrx
d
Hmgn5
Tsc22d3
Bcorl1
RNA levels relative to Rpl13a
Mo/Mφ
spl. DC
spl. B
spl. T
3-mos WT
3-mos Ftx KO
1-yr WT
1-yr Ftx KO

Sup 2

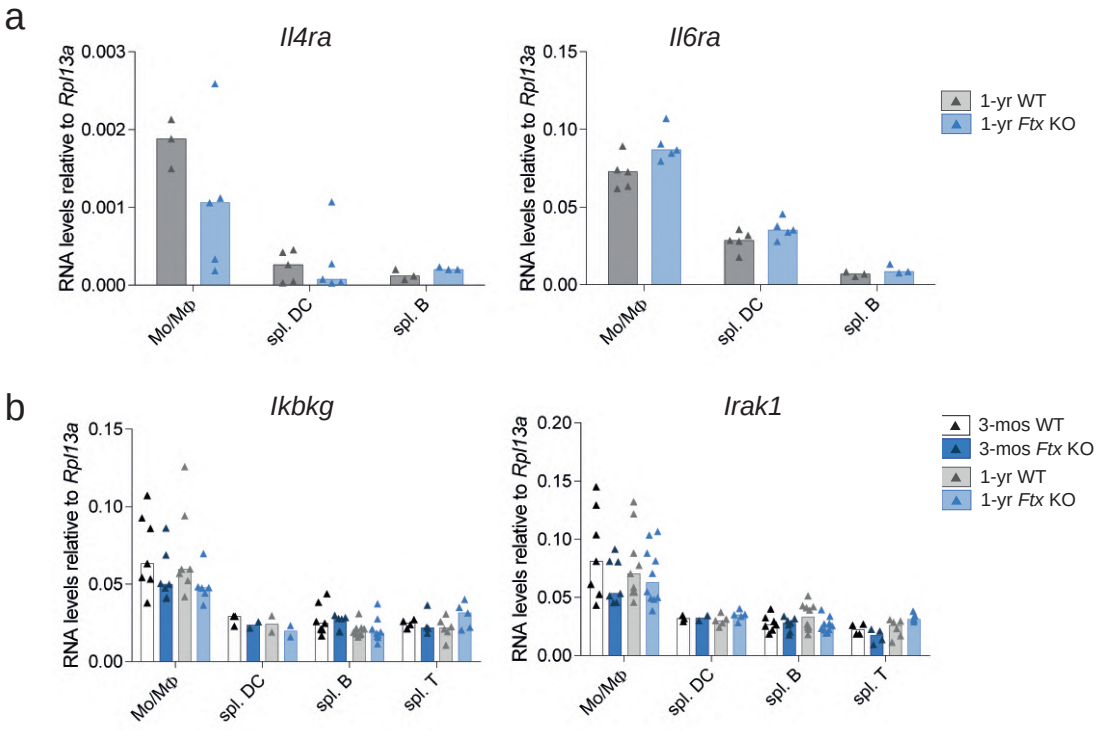
a
Il4ra
Il6ra
RNA levels relative to Rpl13a
0.003
0.002
0.001
0.000
0.15
0.10
0.05
0.00
Mo/Mφ
spl. DC
spl. B
1-yr WT
1-yr Ftx KO
b
Ikbkg
Irak1
0.20
spl. T
3-mos WT
3-mos Ftx KO

Sup 3

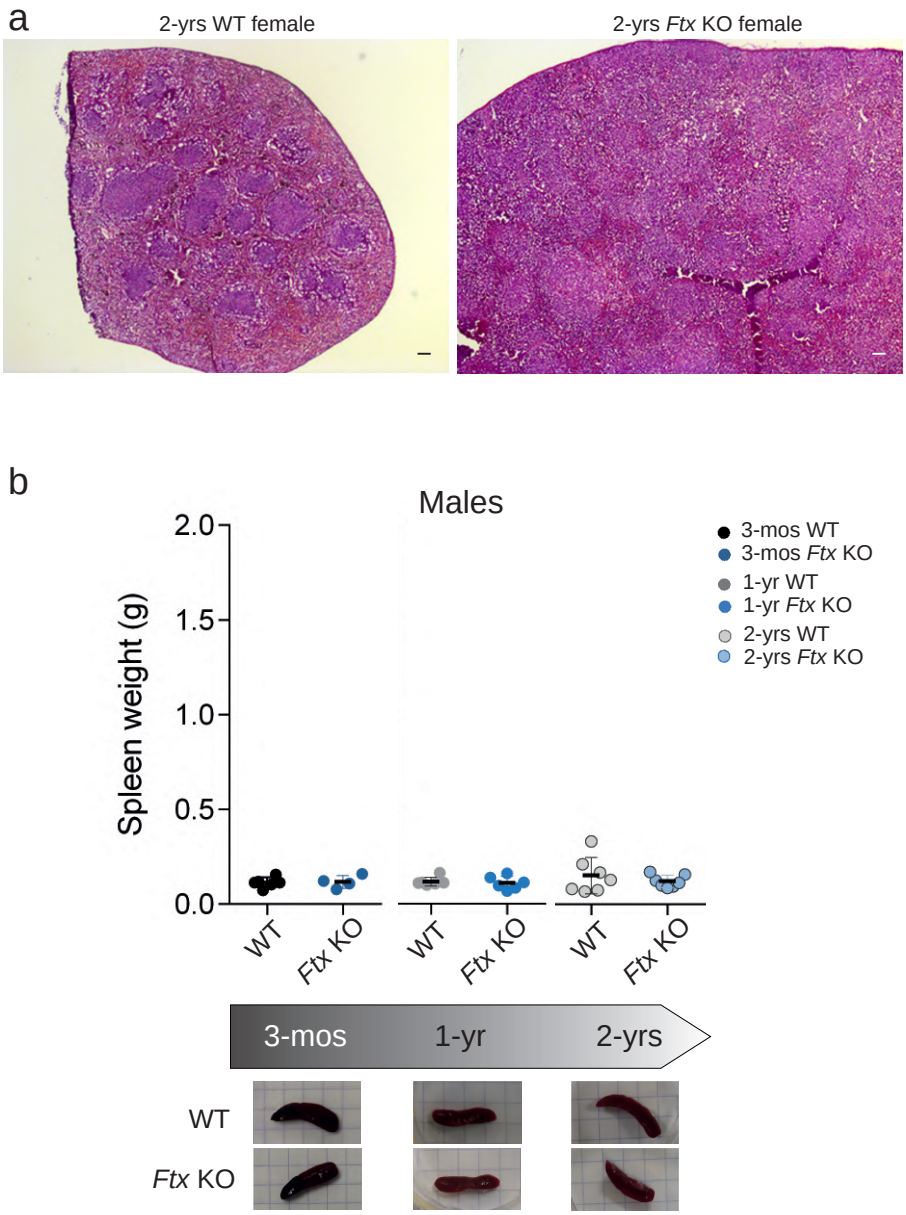
a
2-yrs WT female
2-yrs Ftx KO female
b
Males
Spleen weight (g)
2.0
1.5
1.0
0.5
0.0
3-mos WT
3-mos Ftx KO
1-yr WT
1-yr Ftx KO
2-yrs WT
2-yrs Ftx KO
WT
Ftx KO
WT
Ftx KO
WT
Ftx KO
3-mos
1-yr
2-yrs
WT
Ftx KO

Sup 4

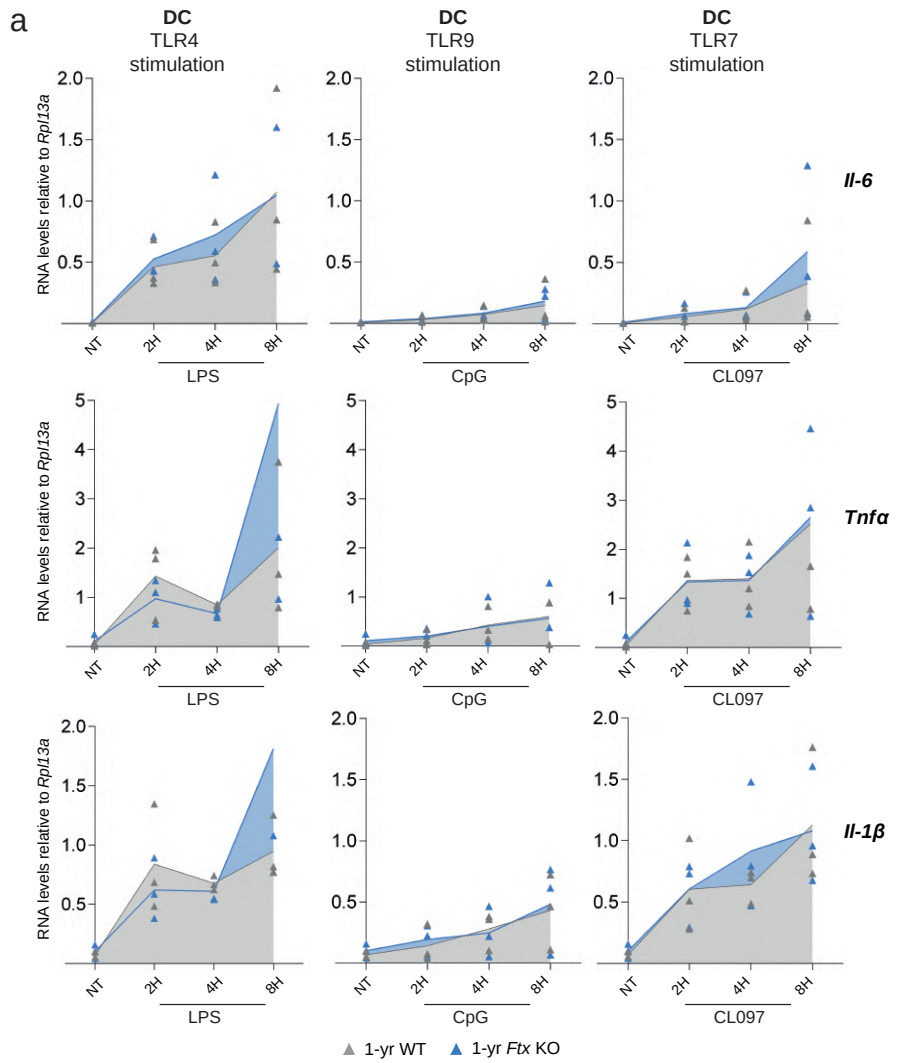
a
DC
TLR4
stimulation
DC
TLR9
stimulation
DC
TLR7
stimulation
RNA levels relative to Rpl13a
Il-6
Tnfα
Il-1β
NT
2H
4H
8H
LPS
CpG
CL097
1-yr WT
1-yr Ftx KO

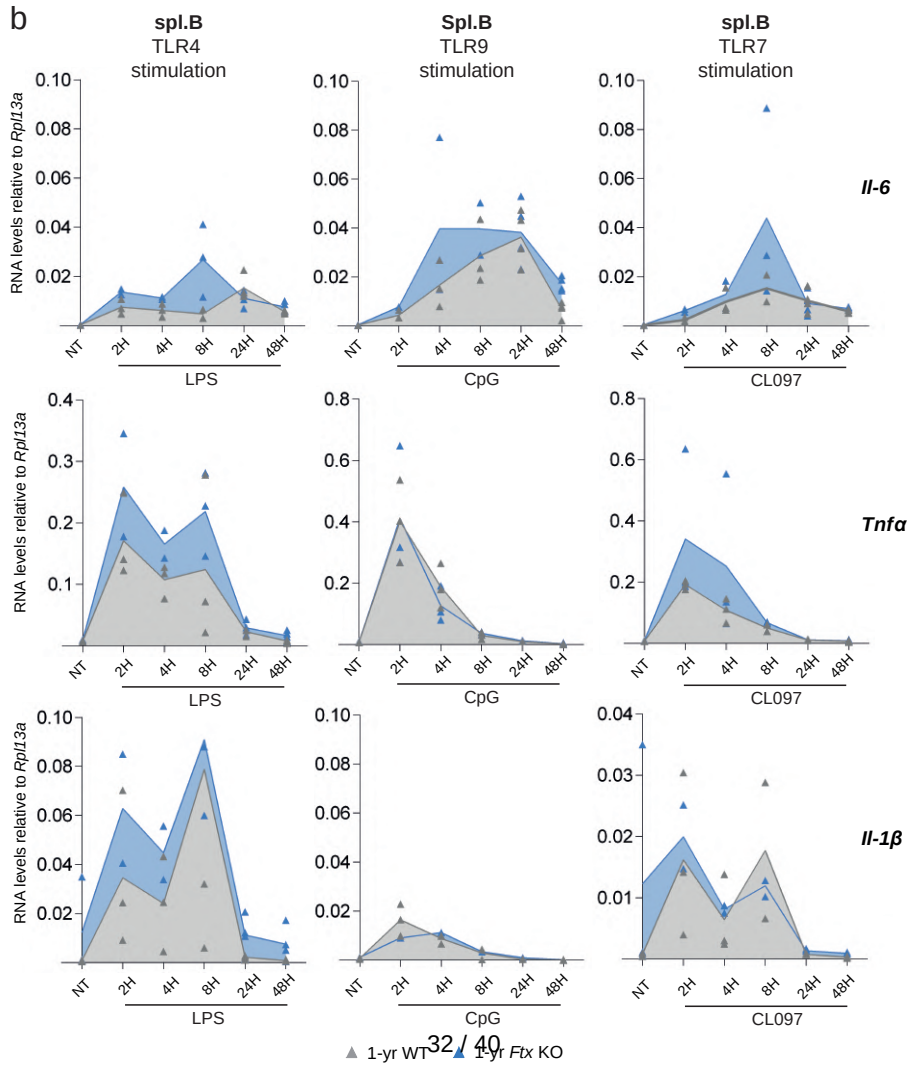
b
spl.B
TLR4
stimulation
Spl.B
TLR9
stimulation
spl.B
TLR7
stimulation
RNA levels relative to Rpl13a
Il-6
Tnfα
Il-1β
NT
2H
4H
8H
24H
48H
LPS
CpG
CL097
1-yr WT
1-yr Ftx KO

Sup 5

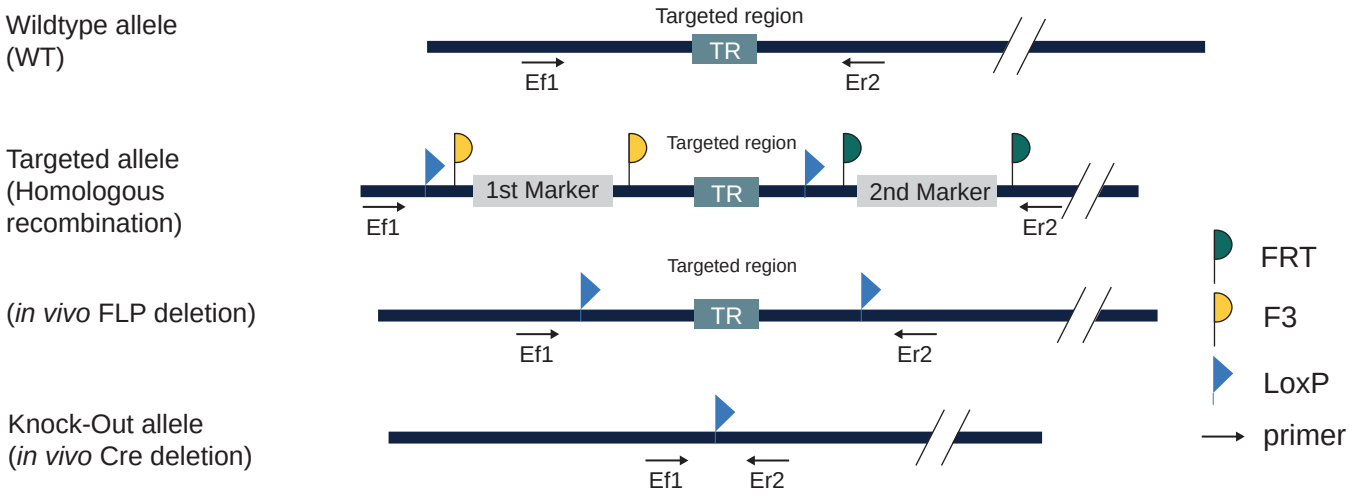
Wildtype allele
(WT)
Targeted region
TR
Ef1
Er2
Targeted allele
(Homologous
recombination)
Targeted region
1st Marker
TR
2nd Marker
Ef1
Er2
(in vivo FLP deletion)
Targeted region
TR
Ef1
Er2
Knock-Out allele
(in vivo Cre deletion)
Ef1
Er2
FRT
F3
LoxP
primer

Sup 6

Sup Table 1. Mating of *Ftx* mutated mice. No statistically significant difference in genotype frequencies compared to expected Mendelian ratios in any of the crosses (c^2 test).

Cross (XX) x (XY)	Male pups		Female pups		Total
(+/+) x (-/Y)	(+/Y)		(+/-)		
	44		36		80
(+/-) x (+/Y)	(+/Y)	(-/Y)	(+/+)	(-/+)	
	160	151	180	150	641
(+/-) x (-/Y)	(+/Y)	(-/Y)	(+/-)	(-/-)	
	89	83	91	87	350
(-/-) x (-/Y)	(-/Y)		(-/-)		
	73		52		125

Sup Table 2. Genes overexpressed in *Ftx* $^{-/-}$ immune cells are enriched in genes associated with autoimmune phenotypes.

Genes analysed in this study	Functional features as in Fig. 1c	Genes overexpressed in this study	Autoimmune disease associated genes	References
Gata1				
Was			Systemic autoimmunity associated with Wiskott-Aldrich syndrome	Libert et al., Nat Rev Immunol., 2010; Becker-Herman et al., J Exp Med., 2010
Foxp3		tendency in T cells (n.s.)	Various autoimmune phenotypes	Mohr et al., Clin Exp Immunol., 2019 and references within
Cybb		Spl. DC	X-linked chronic granulomatous disease	Yu et al., Clin Rev Allergy Immunol., 2021 and references within
Kdm6a			Autoimmune encephalomyelitis	Itoh et al., J Clin Investig., 2019
Upf3b				
Lamp2		tendency in Mo/MΦ (n.s.), tendency in spl. DC (n.s.)	autophagy-related Multiple Sclerosis	Borziak et al., Mult Scler Relat Disord., 2022
Xiap				
Bcorl1				
Elf4				
Cd40Lg		tendency in T cells (n.s.)	SLE, systemic sclerosis, rheumatoid arthritis	Lian et al., Arthritis Rheum., 2012; Lu et al., J Immunol., 2007; Liao et al., Clin Immunol., 2012
Irak1		tendency in T cells (n.s.)	SLE	Su et al., Autoimmunity Rev., 2020 and references within
Ikbkg		tendency in T cells (n.s.)	Systemic autoinflammatory disease	De Jesus et al., J Clin Invest., 2020; Lee et al., J Clin Invest., 2022
G6dpx				
Tasl		Mo/MΦ, tendency in spl. DC (n.s.)	SLE	Odhams et al., Nat Commun., 2019
Pola1				
Msn				
Kif4				
Nono				
Taf1				
Ogt				
Cxcr3		Spl. T	SLE	Wang et al., Proc Natl Acad Sci., 2016
Ercc6l				
Il2rg		Mo/MΦ		
Rlim				
Atrx				
Atp7a		Mo/MΦ		
Tlr13		Mo/MΦ, Spl. DC		
Pgk1				
Itm2a			Various autoimmune phenotypes	Chang et al., PLoS One, 2014
Hmgn5				
Apool				
Btk			Various autoimmune phenotypes	McDonald et al., Immunology, 2021 and references within
Tceal9				
Prps1				
Tsc22d3				
Tmem29				
Kdm5c			SLE	Syrett et al., JCI Insight, 2019
Prdx4				
Pdha1				
Tmsb4x				
Tlr8		Mo/MΦ	Systemic Sclerosis, SLE	Demaria et al., J Clin Invest., 2010
Tlr7		Mo/MΦ, Spl. DC, Spl. B	SLE and other autoimmune manifestations	Deane et al., Immunity, 2007; Wang et al., Front Immunol., 2021
Prps2			SLE	Zhang et al., Hum Mol Genet., 2014

	immune function and tendency to escape from X-inactivation
	constitutively escape from X-inactivation
	housekeeping
	immune function

Sup Table 3. Splenic and BM cell distributions in WT and *Ftx* $^{-/Y}$ male mice.
Values denote percentages (mean ± SD) of nucleated cells except for erythroid cells.
n ≥ 3, t-test versus WT, *p < 0.05; § p <0.01, N.D. not determined.

Spleen	3-mos		1-yr	
	WT	*Ftx* KO	WT	*Ftx* KO
B cells (CD19^{+})	58.1 ± 1.4	53.1 ± 5.7	55.3 ± 8.3	50.0 ± 8.7
MZ B cells (CD19^{+}B220^{+}CD21^{+}CD23^{-})	N.D.	N.D.	3.5 ± 0.9	3.4 ± 1.1
Follicular B cells (CD19^{+}B220^{+}CD21^{int}CD23^{+})	N.D.	N.D.	33.9 ± 11.4	23.9 ± 11.0
Transitional B cells (CD19^{+}B220^{+}CD21^{lo}CD23^{-}IgM^{+})	N.D.	N.D.	2.3 ± 1.3	3.1 ± 2.0
T cells (CD3^{+})	28.5 ± 2.4	27.7 ± 3.7	25.5 ± 4.0	23.9 ± 6.7
Cytotoxic T (CD8^{+}CD4^{-})	N.D.	N.D.	N.D.	N.D.
Helper T (CD8^{-}CD4^{+})	N.D.	N.D.	14.9 ± 2.1	13.0 ± 2.4
Myeloid (CD11b^{+})	8.6 ± 3.0	8.4 ± 2.7	10.1 ± 5.8	9.3 ± 3.6
Mo/MΦ (CD11b^{+}F4/80^{+})	N.D.	N.D.	3.8 ± 1.8	3.2 ± 0.6
Dendritic (CD11c^{+})	N.D.	N.D.	3.9 ± 0.8	3.9 ± 1.0
m-DC (CD11c^{+}CD11b^{+})	N.D.	N.D.	2.4 ± 0.8	1.9 ± 0.15
p-DC (CD11c^{+}B220^{+}SiglecH^{+})	N.D.	N.D.	0.27 ± 0.08	0.29 ± 0.14
Erythroid cells (Ter119^{+})	N.D.	N.D.	44.4 ± 4.7	49.2 ± 10.3
Cell count (x 10^{6})	237 ± 10	232 ± 22	215 ± 110	203 ± 63

Bone Marrow	3-mos		1-yr		2-yr	
	WT	*Ftx* KO	WT	*Ftx* KO	WT	*Ftx* KO
Hematopoietic stem progenitors (Lin^{-}Sca1^{+}ckit^{+})	0.2 ± 0.03	0.15 ± 0.02	N.D.	N.D.	1.5 ± 0.5	1.5 ± 0.7
LT-HSC (LSK^{+}CD34^{-}Flt3^{-}CD150^{+})	0.006 ± 0.001	0.005 ± 0.001	N.D.	N.D.	0.189 ± 0.084	0.151 ± 0.069
ST-HSC (LSK+CD34+Flt3-)	0.046 ± 0.006	0.047 ± 0.006	N.D.	N.D.	0.853 ± 0.436	0.879 ± 0.460
MPP (LSK+CD34+Flt3^{int})	0.032 ± 0.007	0.034 ± 0.007	N.D.	N.D.	0.212 ± 0.088	0.234 ± 0.101
LMPP (LSK+CD34+Flt3^{hi})	0.046 ± 0.013	0.057 ± 0.010	N.D.	N.D.	0.135 ± 0.064	0.181 ± 0.123
B cells (CD19^{+})	23.7 ± 4.4	22.7 ± 1.8	13.2 ± 4.9	14.6 ± 11.3	15.9 ± 9.4	22.4 ± 4.7
proB (CD19^{+}B220^{lo}CD43^{lo})	1.8 ± 0.4	2.2 ± 0.6	N.D.	N.D.	1.7 ± 0.3	2.5 ± 1.8
preB (B220^{lo}CD43^{-}IgM^{-})	9.2 ± 2.6	7.9 ± 1.5	N.D.	N.D.	4.6 ± 1.3	5.1 ± 4.4
Imm. B (B220^{lo}CD43^{-}IgM^{+})	3.9 ± 1.1	3.1 ± 0.3	N.D.	N.D.	3.5 ± 0.3	2.0 ± 1.4
recirc. B (B220^{hi}CD43^{-}IgM^{+})	6.8 ± 1.2	6.6 ± 1.2	N.D.	N.D.	5.1 ± 0.5	3.1 ± 2.5
T cells (CD3^{+})	2.9 ± 0.3	2.8 ± 0.6	9.8 ± 4.5	10.7 ± 4.9	9.3 ± 3.7	11.5 ± 1.7
Myeloid (CD11b^{+})	63.1 ± 5.8	64.1 ± 4.7	66.2 ± 11.7	65.2 ± 4.9	53.7 ± 11.3	44.4 ± 6.3
Mo/MΦ (CD11b^{+}F4/80^{+})	N.D.	N.D.	19.0 ± 2.9	14.9 ± 5.1	N.D.	N.D.
Erythroid cells (Ter119^{+})	N.D.	N.D.	45.7 ± 5.5	43.3 ± 7.6	N.D.	N.D.
Cell count (x 10^{6})	90 ± 3	92 ± 2	60 ± 4	76 ± 4	89 ± 2	104 ± 29

Sup Table 4. B cell distributions in the bone marrow of WT and *Ftx* $^{-/-}$ female mice.
Values denote percentages (mean ± SD) of nucleated cells except for erythroid cells.
n ≥ 4, t-test versus WT, *p < 0.05; § p <0.01, N.D. not determined.

	3-mos		1-yr		2-yr	
	WT	*Ftx* KO	WT	*Ftx* KO	WT	*Ftx* KO
Hematopoietic stem progenitors (Lin$^-$Sca1$^+$ckit$^+$)	0.49 ± 0.25	0.38 ± 0.07	N.D.	N.D.	1.2 ± 0.4	1.5 ± 0.7
LT-HSC (LSK$^+$CD34$^-$Flt3$^-$CD150$^+$)	0.021 ± 0.005	0.016 ± 0.001	N.D.	N.D.	0.104 ± 0.030	0.143 ± 0.089
ST-HSC (LSK+CD34+Flt3-)	0.172 ± 0.118	0.115 ± 0.026	N.D.	N.D.	0.591 ± 0.205	0.840 ± 0.368
MPP (LSK+CD34+Flt3^{int})	0.078 ± 0.026	0.068 ± 0.011	N.D.	N.D.	0.265 ± 0.086	0.291 ± 0.152
LMPP (LSK+CD34+Flt3^{hi})	0.052 ± 0.012	0.060 ± 0.015	N.D.	N.D.	0.187 ± 0.065	0.155 ± 0.076
B cells (CD19$^+$)	23.6 ± 3.8	25.9 ± 5.7	12.8 ± 7.3	10.1 ± 5.4	10.0 ± 2.4	5.2 ± 1.3 §
proB (CD19$^+$B220^{lo}CD43^{lo})	0.52 ± 0.25	0.43 ± 0.18	2.9 ± 1.3	2.2 ± 1.6	1.5 ± 0.6	1.1 ± 0.4 *
preB (B220^{lo}CD43$^-$IgM$^-$)	2.3 ± 0.5	1.9 ± 0.8	2.8 ± 1.6	2.1 ± 2.1	3.2 ± 0.9	3.6 ± 1.7
Imm. B (B220^{lo}CD43$^-$IgM$^+$)	1.3 ± 0.4	1.2 ± 0.4	2.7 ± 1.2	1.0 ± 1.3 *	0.95 ± 0.32	1.33 ± 0.33 *
recirc. B (B220^{hi}CD43$^-$IgM$^+$)	2.4 ± 0.6	2.6 ± 0.8	3.7 ± 2.0	1.4 ± 1.2 *	1.9 ± 0.6	1.2 ± 0.4 *
T cells (CD3$^+$)	5.6 ± 2.2	5.0 ± 0.9	5.9 ± 1.6	5.6 ± 2.5	6.4 ± 1.7	5.7 ± 1.8
Myeloid (CD11b$^+$)	47.3 ± 7.6	45.8 ± 3.3	47.3 ± 8.9	57.8 ± 8.5	38.3 ± 5.3	38.5 ± 5.2
Mo/MΦ (CD11b$^+$F4/80$^+$)	11.3 ± 1.6	9.8 ± 2.2	10.7 ± 1.7	10.6 ± 3.0	N.D.	N.D.
Erythroid cells (Ter119$^+$)	64.7 ± 4.5	65.1 ± 6.0	59.8 ± 8.0	59.4 ± 4.9	N.D	N.D
Cell count (x 10^6)	79 ± 15	71 ± 18	46.7 ± 8	48 ± 13	14 ± 4	15 ± 3

SUP TABLE5. Primer sequences. Orientation 5' to 3'.

Gene Name	Fwd	Rev
Apool	GAACCCAAAAAGCAGCTAGTGA	GATGCAAAGCCCCTTTGTAAAT
Atp7a	AACACCTCTTTTGCCCTCAA	TGCGTTCAATGTTTGCTACA
Atrx	CAAGATCTCGAGGAGGTGGA	AAGACCTAATGTTCTCAGCCAATG
Bcorl1	ACCACAGCCACACGATAAGC	CTGGGGCTTTTCTTGGTGGG
Btk	TGTCCATCAATCCAGAAGCAA	TGAGAAAGCGCTGGATTCAC
Cd40lg	CCTTGCTGAACTGTGAGGAGA	TGCATTTCAAAGCTGTTTTCTTT
Cxcr3	AGGGAGAGGTGCTGTTTTCC	ACCAGCCAAGCCATGTACC
Cybb	CTTCTGAATTGGAAGGAAGGTG	TGACATGCCAGAAGAGGGTAA
Elf4	CCCCACAAGGCTCAGGTTAT	GGGCTGTTGGTTCCTGAAG
Ercc6l	AGCTGCTTCTTTGGCTTCTTG	GGAGGCTTCCCAAGGCTTA
Foxp3	GGAGAAGCTGGGAGCTATGC	TGGCTACGATGCAGCAAGA
Ftx	GCCGCTTTTGAAGAGATAAACT	TGATTATCCTCATGTGTTGCTG
G6pdx	GGCCCTGAAACCCTACAATG	GGACCGCCATTTTGTCCTAT
Gata1	CCGCCAGAGTGTTGTAGTGG	GTCAGAACCGGCCTCTCATC
Hmgn5	ATAAAGGTGTCATGTTAGGCATTTTG	TGCTTTTCTTTAGCATCATTCAATC
Ikbkg	GCCTTAAAGGAGTTGGAGCAA	CTGGAGTTCTCCGAGCAATG
Il-10	AACTGCACCCACTTCCCAGT	TGTCCAGCTGGTCCTTTGTT
Il1b	TGTAGTGCAGTTGTCTAATG	GACATGAGCACCTTCTTT
Il2rg	CCGTTTCAGCTCATCCACAC	GTGCAGTACCGGAGCAACAG
Il4ra	TTTGCCTGTTCTGTTACTTCTCG	CTGGTCCCACCATATCTTCTTAATC
Il-6	TCTGGGAAATCGTGGAAATG	TTTCTGCAAGTGCATCATCG
Il6ra	GCCTCTGACTTCCATTTCTGC	GGGTTGCTTCTCTGTGTCTTCAT
Irak1	GGGTGCTTTTCAGGGTCACT	AGAGGGCTGTGAGGACACAA
Itm2a	TCTTCCACAGCAACCAGGTC	GACTCCAAAGAATCTGGTGGAAC
Kdm5c	GGGAAGCAGGGCTCTGAA	GAGCACAAAGCTAGGGGAAGC
Kdm6a	GTTTGTCTTAATGCAGCAACACCA	TGTTGGCCCATTAAGAATTCCAGT
Kif4	GTGAGGCAGCTGGTCAAACA	CATGCCGCCTGAGTTCTTCT
Lamp2	GGAAGACTGGAAGGTTCAAGAGA	CAAGACACAAGGCAATTCCAA
Msn	TGTGTTGTTTAGGGACAGAAGGAG	TCCTCCAATCGGTACAAAGC
Nono	TGAGAAATATGGAAAAGCAGGCGA	GCATGTTGTCCAGCTCCACT
Ogt	ACAGAGGGCAGATTCAGATAAC	CTCCGGTTGCAGCCTTATTA
Pdha1	CAGAGCCACCAGCATTCCTA	CAAACTTGAAGCCAGCCATCTAC
Pgk1	ACTTTGCCAAGGCTTTGGAG	CCATTCCACCACCAATGATC
Pola1	GCACAGCTGGGTGTACAAGG	CGACGTCTTCCCCTTCATTT
Prdx4	TCTGCCTCAGGACTCCTTTGT	TCTTTCTGACCTGAACCATCAGA
Prps1	CGACCTTCCTTAGCCTACTACCTC	AGTAAGTTCAATTGAGAGGCCAAAC
Prps2	AGTTTAGCAGAAATTGGAG	AGATTAATGACAACCTGATG
Rlim	CACGTTCAGAACGGGAAAAG	TGGAGAATACCGGCAGAGAG
Rpl13a	GGCTGTCATCACTGCCTGGTACT	GCTGCTCTCAAGGTTGTTCG
Taf1	CCTCAGCCAGTGAAAAAGACAG	TCCTCAGGCACACCAAATTTAC
Tasl	TGTTGCTGCAGGATCCAAGG	CCCAGCCACCGGTTCATTAT
Tceal9	CTTTGTACCGCACCAGGCTA	TTTGGCAGGGTTTCATCTTG
Tgfb1	GACTACTATGCTAAAGAGGTCACCC	GCTTCCCGAATGTCTGACGT
Tlr13	CAGAATGAGTGGGCTCTACAGG	TGACTGTCTTAGGCATCCAGGT
Tlr7	CTGAGAAGGGAGCCAAGGAC	TGCGAGTCTCGGTTTTCTGT
Tlr8	CAGCAGACAAAAGCACGTCA	CTTCCAGAAAAACAGAGTTGGATG
Tmem29	GACCAGGACATACAGGAACATC	CTGCTTTCTGGTACTCTCTCAC
Tmsb4x	GTGGAATGTACAGTGCATAT	GCTGAGATCGAGAAATTC
Tnfa	CTGATGAGAGGGAGGCCATT	CAGCCTCTTCTCATTCCTGCT
Tsc22d3	CAGCTCACGAATCTGCTCCTT	TGGTGGCCCTAGACAACAAG
Upf3b	CAGAATAAGATTGCAGGCTCAGA	TCACTTGCAATGTTCTTGCTACC
Was	GCTTGCTGGAAGGAAGATGAC	AGGCCTAGTAGGTGCCCTGA
Xiap	GTGCTCAGAAAGATAATACG	TCTATCCATACAGATTTTGC
Xist	GGTTCTCTCTCCAGAAGCTAGGAAAG	TGGTAGATGGCATTGTGTATTATATGG
Ef1-Er2	GGCTAAGTCATTAGGCAGGTCCAATC	CTACAGCAGACACTAGCTCAGAAGTG

Supplementary material

Sup1. Lack of *Ftx* transcripts in *Ftx* KO immune cells.

- **a.** Map of the mouse X-inactivation center showing the boundaries of the *Ftx* promoter deletion and, underneath, the effect on the various known isoforms of *Ftx* transcripts.
- **b.** RT-qPCR analysis of *Ftx* RNA levels in indicated cell populations collected either from 3-month- or from 1-year-old WT of *Ftx* KO female mice. qPCR yielded no PCR products in KO animals. Each triangle represents a mouse. Bar plots show median values.
- **c.** Double RNA-FISH for *Ftx* (red) and for *Xist* (green) in indicated cell populations collected from 1-year-old WT or *Ftx* KO females. (*Fisher's exact test*; **p-values* < 0.05; N ≥ 2 mice; n ≥ 100 nuclei).

Sup2. Expression levels of individual X-linked genes.

- **a.** Expression of genes known to escape from XCI analysed by RT-qPCR in the indicated cell populations collected either from 3-month- or from 1-year-old WT or *Ftx* KO females. Each triangle represents a mouse. Bar plots show median values. (*t-test*; **p-values* < 0.05).
- **b.** Same as in panel **a** for genes with immune functions.
- **c.** Same as in panel **a** for housekeeping genes.
- **d.** Same as in panel **a** for genes showing a tendency to be expressed at a lower level in *Ftx* KO compared to WT immune cells.

Sup3. Expression levels of autosome-linked *IL4* and *IL6* membrane receptors and of X-linked members of the NF-κB signaling pathway.

- **a.** Expression of autosomal genes encoding cytokine membrane receptors analysed by RT-qPCR in the indicated cell populations collected either from 3-month- or from 1-year-old WT or *Ftx* KO females. Each triangle represents a mouse. Bar plots show median values. (*t-test*; not significant).
- **b.** Same as in panel **a** for X-linked member of the NF-κB pathway, *Ikbkg* (NEMO) and *Irak1*.

Sup4. Morphological and histological analyses of spleens from 2-year-old female and male mice.

- **a.** Hematoxylin-Eosin staining of spleen sections from 2-year-old WT or KO females.
- **b.** Spleen weight of wild-type (WT) and *Ftx* KO males at 3-months, 1-year and 2-years of age. Each triangle represents a mouse. Median values are shown. (*t-test*, not significant). Underneath, representative images of WT and *Ftx* KO spleens from 3-month-, 1-year- and 2-year-old males.

Sup5. Effect of TLR4, TLR9 or TLR7 activation on cytokine expression in BM-derived dendritic cells or in splenic B cells from WT or from *Ftx* KO 1-year-old females.

- **a.** RT-qPCR analysis of cytokine RNA levels in BM-derived dendritic cells (GM-CSF differentiation of total BM cells) activated either with LPS (*TLR4* pathway), CpG (*TLR9* pathway) or with the *TLR7* agonist CL097. Cells were either not treated (NT) or treated for 2, 4, 8 or 24 hours. Each triangle represents a mouse. Median values are shown. (*t-test*, not significant).
- **b.** Same as in panel **a** in splenic B cells.

Sup6. Strategy used to generate the *Ftx* deficient mouse line.

Independent targeted C57BL/6N ES cell lines, were injected into C57BL/6N blastocysts to create germline chimeras. The targeted allele derived from recombinant ES cells was transmitted to female offspring from chimeric males. Mice carrying *Ftx* promoter deletion were obtained after two-rounds of *in vivo* recombination with FLP and Cre driver mice successively resulting in a single *LoxP* site left at the position of the deleted region. Ef1 and Er2 primer pair was used for PCR genotyping.